Dilepton Production from AGS to SPS Energies within a Relativistic Transport Approach *

E. L. Bratkovskaya and W. Cassing
Institut für Theoretische Physik, Universität Giessen
D-35392 Giessen, Germany

Abstract

We present a nonperturbative dynamical study of e^+e^- production in proton-nucleus and nucleus-nucleus collisions from AGS to SPS energies on the basis of the covariant transport approach HSD. For p + Be reactions the dilepton yield for invariant masses $M \leq 1.4$ GeV is found to be dominated by the decays of the η, ρ, ω and Φ mesons at all energies from $10 - 450$ GeV. For nucleus-nucleus collisions, however, the dilepton yield shows an additional large contribution from $\pi^+\pi^-$, K^+K^- and $\pi\rho$ channels. Systematic studies are presented for the 'free' meson mass scenario in comparison to a 'dropping' meson mass scenario at finite baryon density. We find that for 'dropping' meson masses the invariant dilepton mass range 0.35 GeV $\leq M \leq$ 0.65 GeV is increased in comparison to the 'free' meson mass scenario and that the data of the CERES-collaboration for nucleus-nucleus collisions can be described much better within the 'dropping' mass scheme. We study in detail the contributions from the various dilepton channels as a function of the transverse momentum and rapidity of the lepton pair as well as a function of the charged particle multiplicity. Furthermore, various direct photon channels for S + Au at 200 GeV/u are computed and found to be well below the upper bounds measured by the WA80-collaboration.

PACS: 25.75+r 14.60.-z 14.60.Cd
Keywords: relativistic heavy-ion collisions, leptons

---

1 Introduction

The question of chiral symmetry restoration at high baryon density is of fundamental interest since a couple of years [1, 2], but a clear experimental evidence has not been achieved, so far. The enhancement of strangeness production as e.g. seen in the AGS data for the K^+/π^+ ratio [3] might be a signiture for such a transition [4], however, other hadronic scenarios can be cooked up to describe this phenomenon as well [5]. Enhanced antikaon yields at SIS energies, as compared to transport studies using bare kaon masses [6, 7], point in the same direction, but here the present knowledge on the elementary production cross sections close to threshold does not yet allow for a final identification. On the other hand, dileptons are particularly well suited for an investigation of the violent phases of a high-energy heavy-ion collision because they can leave the reaction volume essentially undistorted by final-state interactions. Indeed, dileptons from heavy-ion collisions have been observed by the DLS collaboration at the BEVALAC [8, 9, 10] and by the CERES [11], HELIOS [12, 13], NA38 [14] and NA50 collaborations [15] at SPS energies.

Quite some years ago it has been found within microscopic transport studies at BEVALAC/SIS energies [16, 17] that above about 0.5 GeV of invariant mass (of the lepton pair) the dominant production channel is from $\pi^+\pi^-$ annihilation, such that the properties of the short lived ρ meson could be explored at high baryon density. The data available so far, however, did not allow for a closer distinction of the various models proposed.

The recent data on e^+e^- or $\mu^+\mu^-$ spectra at SPS energies, on the other hand, are more conclusive. The enhancement of the low mass dimuon yield in S + W compared to p + W collisions [12] at 200 GeV/u has been first suggested by Koch et al. [18] to be due to $\pi^+\pi^-$ annihilation. Furthermore, Li et al. [19] have proposed that the enhancement of the e^+e^- yield in S + Au collision as observed by the CERES collaboration [11] should be due to an enhanced ρ-meson production (via $\pi^+\pi^-$ annihilation) and a dropping ρ-mass in the medium. In fact, their analysis – which was based on an expanding fireball scenario in chemical equilibrium – could be confirmed within the microscopic transport calculations in Ref. [20]. Meanwhile, various authors have substantiated the observation in Refs. [19, 20], that the spectral shape of the dilepton yield is incompatible with 'free' meson form factors [21, 22, 23]. However, a more conventional approach including the change of the ρ-meson spectral function in the medium due to the coupling of the ρ, π, Δ and nucleon dynamics along the line of Refs. [24, 25, 26] was found to be roughly compatible with the CERES data [20, 27], too. On the other hand, the dimuon data of the HELIOS-3 collaboration [12] could only be described satisfactorily when including 'dropping' meson masses [28, 29].

Though meanwhile there are a couple of hints on 'dropping' meson masses with baryon density and thus on a partial restoration of chiral symmetry for very hot and dense nuclear matter, a more systematic study of medium effects on the differential dilepton spectra – also with respect to the transverse momentum p_T and rapidity y – appears necessary to optimize the experimental setups.

Our paper is organized as follows: we start with a brief reminder of the covariant transport approach employed in our analysis in Sect. 2 and present the actual

expressions and form factors used for the evaluation of the differential dilepton multiplicities. In Sect. 3 we investigate the question, at which bombarding energies one might find optimal conditions for high baryon densities at sufficiently large timescales in Pb + Pb collisions. Section 4 contains the comparison of our calculated dilepton spectra for p + Be and Pb + Au reactions with experimental data at SPS energies. Detailed predictions for dilepton production form AGS to SPS energies will be presented in Sect. 5 for p + Be and Pb + Pb collisions within the 'free' and 'dropping' meson mass scenario. Section 6 concentrates on direct photon production in S + Au collisions at 200 GeV/u, while Section 7 concludes our study with a summary and discussion of open problems.

2   The covariant transport approach

In this paper we perform our analysis along the line of the HSD[1] approach [4] which is based on a coupled set of covariant transport equations for the phase-space distributions $f_h(x,p)$ of hadron h [4, 30], i.e.

$$\left\{ \left(\Pi_\mu - \Pi_\nu \partial^p_\mu U^\nu_h - M^*_h \partial^p_\mu U^S_h \right) \partial^\mu_x + \left(\Pi_\nu \partial^x_\mu U^\nu_h + M^*_h \partial^x_\mu U^S_h \right) \partial^\mu_p \right\} f_h(x,p)$$

$$= \sum_{h_2 h_3 h_4 \dots} \int d2d3d4 \dots [G^\dagger G]_{12 \to 34 \dots} \delta^4(\Pi + \Pi_2 - \Pi_3 - \Pi_4 \dots)$$

$$\times \left\{ f_{h_3}(x,p_3) f_{h_4}(x,p_4) \bar{f}_h(x,p) \bar{f}_{h_2}(x,p_2) \right.$$

$$\left. - f_h(x,p) f_{h_2}(x,p_2) \bar{f}_{h_3}(x,p_3) \bar{f}_{h_4}(x,p_4) \right\} \dots \quad . \tag{1}$$

In Eq. (1) $U^S_h(x,p)$ and $U^\mu_h(x,p)$ denote the real part of the scalar and vector hadron selfenergies, respectively, while $[G^+G]_{12\to 34\dots}\delta^4_\Gamma(\Pi+\Pi_2-\Pi_3-\Pi_4\dots)$ is the 'transition rate' for the process $1+2 \to 3+4+\dots$ which is taken to be on-shell in the semiclassical limit adopted. The hadron quasi-particle properties in (1) are defined via the mass-shell constraint [30],

$$\delta(\Pi_\mu \Pi^\mu - M^{*2}_h) \quad , \tag{2}$$

with effective masses and momenta given by

$$\begin{aligned} M^*_h(x,p) &= M_h + U^S_h(x,p) \\ \Pi^\mu(x,p) &= p^\mu - U^\mu_h(x,p) \quad , \end{aligned} \tag{3}$$

while the phase-space factors

$$\bar{f}_h(x,p) = 1 \pm f_h(x,p) \tag{4}$$

are responsible for fermion Pauli-blocking or Bose enhancement, respectively, depending on the type of hadron in the final/initial channel. The dots in Eq. (1) stand for further contributions to the collision term with more than two hadrons in the final/initial channels. The transport approach (1) is fully specified by $U^S_h(x,p)$ and $U^\mu_h(x,p)$ ($\mu = 0, 1, 2, 3$), which determine the mean-field propagation of the hadrons, and by the transition rates $G^\dagger G \, \delta^4(\dots)$ in the collision term, that describes the scattering and hadron production/absorption rates.

---

[1]Hadron String Dynamics

2.1 Hadron selfenergies

The scalar and vector mean fields U_h^S and U_h^μ for baryons are taken from Ref. [4] and don't have to be specified here again, since variations in the baryon selfenergies within the constraints provided by experimental data were found to have no sizeable effect on the dilepton differential spectra. In the present approach we propagate explicitly – apart from the baryons (cf. [4]) – pions, kaons, η's, η''s the 1^- vector mesons ρ, ω, Φ and K^*'s as well as the axial vector meson a_1. We assume that the pions as Goldstone bosons do not change their properties in the medium; we also discard selfenergies for the η and η'-mesons in the present calculation, since we did not find any appreciable selfenergy effects in comparison to the experimental spectra available in the energy regime of interest here.

The kaon selfenergies are described as in Ref. [4] following Kaplan and Nelson [31], i.e. the kaon masses (K^+, K^0) are assumed not to be changed in the medium due to an approximate cancellation of attractive scalar and repulsive vector interactions, whereas the antikaons drop in mass according to

$$m_{\bar{K}}^* = m_{\bar{K}}^0 \left(1 - \lambda_{\bar{K}} \frac{\rho_B}{\rho_0} \right) \geq (m_u + m_s) \approx 0.16 \text{ GeV} \tag{5}$$

with $\lambda_{\bar{K}} \approx 0.16$ as in Ref. [4]. In (5) $m_{\bar{K}}^0$ and $\rho_0 \approx 0.16 \text{ fm}^{-3}$ denote the vacuum antikaon mass and the saturation density of nuclear matter, respectively. Due to a lack of further knowledge about the K^* vector mesons we assume the same scaling with baryon density as for the kaons[2].

The in-medium properties of the vector mesons ρ, ω and Φ are modelled according to the QCD sum rule analysis by Hatsuda and Lee [32] as in our previous studies, i.e.

$$m_V^* = m_V^0 \left(1 - \lambda_V \frac{\rho_B}{\rho_0} \right) \geq (m_u + m_d) \approx 0.016 \text{ GeV} \tag{6}$$

with $\lambda_V \approx 0.18$ for ρ and ω, while the Φ meson is expected to scale with $\lambda_V \approx 0.025$. In line with (6) the in-medium Φ mass is limited to twice the strange quark mass, i.e. $m_\Phi \geq 2m_s \approx 0.3 \text{ GeV}$.

In addition to our previous works [4, 20, 28, 33] we now also include the axial vector meson a_1, i.e. the chiral partner of the ρ meson. Since the scaling of the a_1 mass with baryon density is quite a matter of debate and we only know that $m_{a_1}^* = m_\rho^*$ in the chiral limit, we assume the a_1 to scale in mass in the same way as the ρ meson according to Eq. (6) in order not to introduce any new parameter.

In the following, the 'free' meson mass scenario will employ the limit $\lambda_{\bar{K}} = \lambda_V = \lambda_{a_1} = 0$, whereas the 'dropping' mass scenario is described by Eqs. (5) and (6), respectively.

2.2 Dilepton channels

In this analysis we calculate dilepton production by taking into account the contributions from the Dalitz-decays $\eta \to \gamma e^+ e^-$, $\omega \to \pi^0 e^+ e^-$, $\eta' \to \gamma e^+ e^-$, $a_1 \to \pi e^+ e^-$ and

---

[2]This working hypothesis needs to be controlled in future.

the direct dilepton decays of the vector mesons ρ, ω, Φ where the ρ, Φ and a_1 mesons may as well be produced in $\pi\pi$, $K\bar{K}$ and $\pi\rho$ collisions, respectively.

In case of a perturbative treatment[3] of the channel $\pi^+\pi^- \to \rho^0 \to e^+e^-$ the cross section is parametrized as in Refs. [16, 35, 36] by

$$\sigma_{\pi^+\pi^-\to e^+e^-}(M) = \frac{4\pi}{3} \frac{\alpha^2}{M^2} \sqrt{1 - \frac{4m_\pi^2}{M^2}} |F_\pi(M)|^2, \tag{7}$$

where the 'free' form factor of the pion is approximated by

$$|F_\pi(M)|^2 = \frac{m_\rho^4}{(M^2 - m_\rho{}^2)^2 + m_\rho^2\Gamma_\rho^2}. \tag{8}$$

In Eq. (7) M is the dilepton invariant mass, α is the fine structure constant, and

$$m_\rho = 775 \text{ MeV}, \quad \Gamma_\rho = 118 \text{ MeV}.$$

The cross section for K^+K^- annihilation is parametrized as [37]

$$\sigma_{K^+K^-\to e^+e^-}(M) = \frac{4\pi}{3} \left(\frac{\alpha}{M}\right)^2 \sqrt{1 - \frac{4m_K^2}{M^2}} |F_K(M)|^2, \tag{9}$$

where the 'free' form factor of the kaon is approximated by

$$|F_K(M)|^2 = \frac{1}{9}\frac{m_\Phi^4}{(M^2 - m_\Phi^2)^2 + m_\Phi^2\Gamma_\Phi^2} \tag{10}$$

with

$$m_\Phi = 1020 \text{ MeV}, \quad \Gamma_\Phi = 4.43 \text{ MeV}.$$

The cross section for dilepton production in $\pi^+\rho^- \to \Phi \to e^+e^-$, $\pi^-\rho^+ \to \Phi \to e^+e^-$ scattering can be represented as

$$\sigma_{\pi\rho\to\Phi\to e^+e^-}(M) = \frac{1}{3} \frac{B_{\rho\pi}}{B_{K^+K^-}} \sigma_{K^+K^-\to\Phi\to e^+e^-} \tag{11}$$

with $B_{\rho\pi} = 0.13$, $B_{K^+K^-} = 0.49$.

The η Dalitz decay is given by [38]:

$$\frac{d\Gamma_{\eta\to\gamma e^+e^-}}{dM} = \frac{4\alpha}{3\pi} \frac{\Gamma_{\eta\to 2\gamma}}{M} \left(1 - \frac{4m_e^2}{M^2}\right)^{1/2} \left(1 + 2\frac{m_e^2}{M^2}\right)$$

$$\times \left(1 - \frac{M^2}{m_\eta^2}\right)^3 |F_{\eta\to\gamma e^+e^-}(M)|^2, \tag{12}$$

where the form factor is parametrized in the pole approximation as

$$F_\eta(M) = \left(1 - \frac{M^2}{\Lambda_\eta^2}\right)^{-1}, \tag{13}$$

_____

[3]The perturbative treatment is used to test the dynamical scheme described below in case of the bare ρ-mass scenario, only.

with the cut-off parameter $\Lambda_\eta \simeq 0.72$ GeV.

Similarly, the ω Dalitz-decay is [38]:

$$\frac{d\Gamma_{\omega\to\pi^0 e^+ e^-}}{dM} = \frac{2\alpha}{3\pi} \frac{\Gamma_{\omega\to\pi^0\gamma}}{M} \left(1 - \frac{4m_e^2}{M^2}\right)^{1/2} \left(1 + 2\frac{m_e^2}{M^2}\right)$$
$$\times \left[\left(1 + \frac{M^2}{m_\omega^2 - m_\pi^2}\right)^2 - \frac{4m_\omega^2 M^2}{(m_\omega^2 - m_\pi^2)^2}\right]^{3/2} |F_{\omega\to\pi^0 e^+ e^-}(M)|^2, \qquad (14)$$

where the form factor squared is parametrized as

$$|F_{\omega\to\pi^0 e^+ e^-}(M)|^2 = \frac{\Lambda_\omega^4}{(\Lambda_\omega^2 - M^2)^2 + \Lambda_\omega^2\Gamma_\omega^2} \qquad (15)$$

with

$$\Lambda_\omega = 0.65 \text{ GeV}, \quad \Gamma_\omega = 75 \text{ MeV}.$$

For $\eta' \to \gamma e^+ e^-$ we use a similar expression as Eq. (12). However, in this case the pole approximation (13) is no longer valid since the vector meson pole occurs in the physical region of the dilepton spectrum ($M < m_{\eta'}$). Instead we use a form factor of the form (15) with

$$\Lambda_{\eta'} = 0.75 \text{ GeV}, \quad \Gamma_{\eta'} = 0.14 \text{ GeV},$$

which reproduces the experimental data from [38] reasonably well.

The direct decays of the vector mesons ω, Φ to $e^+ e^-$ are taken as

$$\frac{d\sigma}{dM^2}(M) = \frac{1}{\pi} \frac{m_V \Gamma_V}{(M^2 - m_V^2)^2 + m_V^2\Gamma_V^2} \frac{\Gamma_{V\to e^+ e^-}}{\Gamma_V} \qquad (16)$$

with $\Gamma_{\Phi\to e^+ e^-}/\Gamma_\Phi = 2.5 \times 10^{-4}$ and $\Gamma_{\omega\to e^+ e^-}/\Gamma_\omega = 7.1 \times 10^{-5}$.

The dilepton channels $\eta \to e^+ e^-$, $\omega \to \pi^0 e^+ e^-$, $\omega \to e^+ e^-$, $\Phi \to e^+ e^-$, $\pi\rho \to \Phi \to e^+ e^-$ and $K^+ K^- \to \Phi \to e^+ e^-$ are treated perturbatively and are computed at the end of the transport calculation due to the 'long' lifetime of the mesons $\eta, \eta', \omega, \Phi$. The decays of the short-lived ρ and a_1 mesons, however, have to be treated explicitly since these mesons change their properties rapidly (in case of the dropping mass scenario) and decay during the expansion phase of the system.

The mesons (ρ, a_1) stemming from a string decay with invariant mass m_V^* at baryon density ρ_B according to Eq. (6) are selected by Monte Carlo according to the Breit-Wigner distribution:

$$f(M) = N_V \frac{2}{\pi} \frac{M m_V^* \Gamma_V^*}{(M^2 - m_V^{*2})^2 + m_V^{*2}\Gamma_V^{*2}}, \qquad (17)$$

where N_V guarantees normalization to unity, i.e. $\int f(M)dM = 1$. The width $\Gamma_V^*(M)$ is determined from

$$\Gamma_V^*(M) = \Gamma_0 \left(\frac{m_V^*}{M}\right)^2 \frac{q}{q_V}, \qquad (18)$$

where Γ_0 is the full width at the mean resonance energy, q and q_V are the pion three-momenta in the restframe of the resonance with mass M and m_V^*, respectively.

Apart from string decay the mesons (ρ, a_1) are abundantly also created from $\pi\pi$ or $\pi\rho$ collisions, respectively. For the a_1 formation cross section in the reaction $\pi^+\rho^- \to a_1, \pi^-\rho^+ \to a_1$ or for the ρ^0 cross section the reaction $\pi^+\pi^- \to \rho^0$ we use the Breit-Wigner form [39, 40]:

$$\sigma_V(s) = \frac{2J_V+1}{2S+1} \frac{4\pi}{k^2} \frac{m_V^{*2}\Gamma_V^{*2}}{(s-m_V^{*2})^2 + m_V^{*2}\Gamma_V^{*2}}, \tag{19}$$

where k is the pion momentum in the center-of-mass of the produced meson $V = (\rho, a_1)$, s is the invariant energy squared while J_V stands for the spin of the produced meson and S for the spin of the collision partner of the pion, respectively. In the time reversed processes the vector mesons of actual mass M may decay in each timestep according to the probability

$$P = \exp(-\Gamma_V^*(M)/\gamma\Delta t) \tag{20}$$

where Δt is the actual timestep size and γ the Lorentz factor of the resonance with respect to the calculational frame.

The ρ^0 decay to e^+e^- with invariant mass M is calculated by integrating the equation (using the mass bin ΔM)

$$\frac{dN_{e^+e^-}^\rho}{\Delta M dt} = \frac{1}{\hbar} \sum_{\text{events } i=1}^{N_{\rho^0}(M,t)} \Gamma_{\rho^0 \to e^+e^-}(M) \frac{1}{\Delta M} \tag{21}$$

in time with

$$\Gamma_{\rho^0 \to e^+e^-}(M) = 8.8 \times 10^{-6} \, M, \tag{22}$$

where $N_{\rho^0}(M,t)$ is the number of ρ^0 mesons of mass M at time t in the calculation. The factor 8.8×10^{-6} stems from the measured width of the ρ^0 to e^+e^-. It can be shown [37] that the method described above leads to the same result as Eq. (7) if the ρ^0 meson does not change its properties in time. We note that by treating explicitly the ρ formation by $\pi\pi$ collisions the perturbative channel (7) has been switched off to avoid double counting.

The a_1 decay to πe^+e^- with invariant mass M is calculated in analogy by integrating the equation

$$\frac{dN_{e^+e^-}^{a_1}}{dM dt} = \frac{1}{\hbar} \sum_{\text{events } i=1}^{N_{a_1}(t)} \frac{d\Gamma_{a_1 \to \pi e^+e^-}}{dM}(m_{a_1}^*, M) \tag{23}$$

in time with

$$\frac{d\Gamma_{a_1 \to \pi e^+e^-}}{dM}(m_{a_1}^*, M) = \frac{2\alpha}{3\pi} \frac{\Gamma_{a_1 \to \pi\gamma}}{M} \left(1 - \frac{4m_e^2}{M^2}\right)^{1/2} \left(1 + 2\frac{m_e^2}{M^2}\right)$$

$$\times \left[\left(1 + \frac{M^2}{m_{a_1}^{*2} - m_\pi^2}\right)^2 - \frac{4m_{a_1}^{*2}M^2}{(m_{a_1}^{*2} - m_\pi^2)^2}\right]^{3/2} \tag{24}$$

7

with $\Gamma_{a_1 \to \pi\gamma} = 6.4 \times 10^{-4}$ GeV, while $N_{a_1}(t)$ is the number of a_1 mesons at time t in the calculation.

We note that we discard baryon-baryon (BB), meson-baryon (mB) and meson-meson (mm) bremsstrahlung channels as well as the Dalitz decays of the baryon resonances since their contribution was found to be small in Refs. [20, 28].

Before going over to the actual calculations for e^+e^- spectra, we start with some more general analysis of central heavy-ion collisions from $1 - 200$ GeV/u.

3   Optimizing for high baryon density

In order to probe the restoration of chiral symmetry at high baryon density in nucleus-nucleus collisions, one has to perform experiments with heavy nuclei (e.g. Pb + Pb) and optimize the beam energy to achieve a large volume of high baryon density for a sufficiently long time. In this respect central collisions of Pb + Pb have been investigated within the transport approach specified above and the 'stopped' baryon density $\rho_B^s(t)$ – including only baryons with rapidity $|y| \leq 0.7$ in the cms – has been computed in a central cylinder of the volume $V = \pi R^2 \Delta_z / \gamma_{cm}$ with $\Delta_z = R = 4$ fm, while γ_{cm} is the Lorentz factor in the nucleus-nucleus center-of-mass system. Since we are interested in high baryon densities above some value ρ_{min} for long times, we consider the quantity

$$F = \int dt \, (\rho_B^s(t) - \rho_{min}) \, \Theta(\rho_B^s(t) - \rho_{min}), \qquad (25)$$

which should serve as a useful guide in the optimization problem. The quantity F (Eq. (25)) is displayed in Fig. 1 for central collisions of Pb + Pb from $1 - 200$ GeV/u for different values of ρ_{min} from $2\rho_0 - 5\rho_0$ ($\rho_0 \approx 0.168$ fm^{-3}). Accordingly, optimal bombarding energies for baryon densities above $4\rho_0$ should be around $20 - 30$ GeV/u in order to explore the properties of an intermediate phase, where the chiral symmetry might approximately be restored and the hadron masses (except for the Goldstone bosons) might be close to their current quark masses $m_q + m_{\bar{q}}$. However, also lower bombarding energies ($2 - 10$ GeV/u) are seen to qualify for studies of a partial restoration of chiral symmetry since sizeable space-time volumes with baryon densities above $2 - 3 \, \rho_0$ can be achieved.

Whereas the HSD approach has been shown in Ref. [4] to reasonably reproduce hadronic spectra and rapidity distributions for heavy-ion collisions at SIS and AGS energies, a definite proof for heavy systems at SPS energies is still lacking though quantitative predictions for the baryon rapidity distribution in Pb + Pb collisions at 158 GeV/u have been given in Ref. [4]. In order to demonstrate, that the analysis presented in Fig. 1 is meaningful also at higher bombarding energy, we compare in Fig. 2 the preliminary rapidity distribution of negative hadrons (essentially π^-, K^- and $\bar{p}$) from NA49 [41] for central Pb + Pb collisions at 160 GeV/u with the HSD results. Here the solid line corresponds to a calculation (at $b = 2$ fm) including the 'dropping' meson masses from Eqs. (5), (6), whereas the dotted line results from a calculation with bare meson masses. The broadening of the rapidity distribution around midrapidity ($y \approx 3$) in the 'dropping' mass scenario is due to pions from ρ

and ω decays, which are produced with a wider distribution in rapidity in this case. The quantitative agreement with the data, however, indicates that both scenarios – i.e. 'free' and 'dropping' meson masses as described above – are compatible with the present preliminary data. We note that the open squares in Fig. 2 have been obtained by reflecting the full squares (from NA49) at midrapidity. The fact, that the calculated spectrum is not fully symmetric with respect to midrapidity, is caused by the finite statistics of the computation, which was performed with 150 parallel runs in this case.

Since the system Pb + Pb at 160 GeV/u is explored experimentally at the SPS in great detail, it is advantages to have a look at the space-time evolution of the baryon one-body density for central collisions. In this respect we show in Fig. 3 the space-time evolution of baryons for this system at $b = 0$ fm: (l.h.s.) countor plot of the baryon density distribution in coordinate space $\rho_B(x, y = 0, z; t)$, (middle colum) contour plot of the baryon momentum distribution $\rho_B(p_x, p_y = 0, p_z; t)$, (r.h.s.) the phase-space distribution

$$f(z, p_z; t) = (2\pi)^{-2} \sum_b \int dr_\perp dp_\perp \ f_b(r_\perp, z, p_\perp, p_z; t), \qquad (26)$$

where $\sum_b$ denotes a sum over all baryon species. In the time evolution of the density distribution $\rho_B(x, y = 0, z; t)$ we explicitly mention the short phase of high baryon density from about $5 - 8$ fm/c as well as the sizeable fraction of 'spectators' from the nuclear corona. The time evolution in momentum space (middle colum) shows that the system reaches its final distribution within a few fm/c, however, is far from the kinetic equilibrium in the baryon degrees of freedom, which would be reflected by a spherical distribution here. It clearly indicates a dominant longitudinal expansion of the system, which is much more pronounced than at AGS energies (cf. Fig. 21 in [4]).

4 Comparison with experimental dilepton data at SPS energies

The covariant transport approach HSD has been applied already to the analysis of dilepton spectra for p + Be and Ca + Ca collisions at BEVALAC/SIS energies [42], for p + Be, p + Au, and S + Au collisions at SPS energies [20] and to dimuon spectra for p + W and S + W at 200 GeV/u [12] in Ref. [28]. Whereas the dilepton spectra for p + A reactions at high energy could be well described by the mesonic decays in line with the experimental analysis [11], the S + A data could only be satisfactorily reproduced within the 'dropping' mass scenario (cf. also [19, 29]). Here, we include additional reaction channels (e.g. the η', a_1 degrees of freedom) and present a systematic study with respect to differential spectra in the transverse momentum of the lepton pair, the rapidity distribution as well as the dilepton yield as a function of the charged particle multiplicity at midrapidity. Before doing so, we present the actual status of our calculations in comparison with presently available data on dilepton production at SPS energies.

4.1 Differential dilepton spectra for p + Be and Pb + Au at SPS energies

As an example for dilepton spectra at SPS energies Fig. 4 shows the spectral decomposition as a function of the e^+e^- invariant mass M for p + Be at 450 GeV/c in comparison to the data of the CERES collaboration [11]. The e^+, e^- acceptance cuts in pseudo-rapidity ($2.1 \leq \eta \leq 2.65$), a cut of the transverse e^+ and e^- momenta for $p_T \geq 0.05$ GeV/c as well as a cut on the opening angle of the e^+e^- pair ($\Theta \geq 35$ mrad) are taken into account. Furthermore, the experimental mass resolution has been included in evaluating the final mass spectrum, which is normalized by the number of charged particles $dn_{ch}/d\eta$ in the pseudorapidity bin $2.1 \leq \eta \leq 3.1$. As can be extracted from Fig. 4, the spectrum for p + Be can be fully accounted for by the electromagnetic decays of the η, η', a_1 and vector mesons ρ^0, ω and Φ; contributions from meson-meson channels ($\pi^+\pi^-, K^+K^-, \pi\rho$) are of minor importance here. We note that in our present analysis the a_1 and η' Dalitz decays have been taken into account in addition to Ref. [20]. The η' contribution is more sensitive to the electromagnetic form factor then η or ω Dalitz decays because the vector meson pole shows up in the region $M \leq m_{\eta'}$. However, the contribution of the η' Dalitz decays is not essential compared to the other channels; the a_1 contribution is practically negligible for p + Be.

The situation changes quite dramatically when going over to nucleus-nucleus collisions. In Fig. 5 we compare the results of our calculation for the differential dilepton spectra for Pb + Au at 160 GeV/u at $b = 5$ fm with the preliminary experimental data [43]. Contrary to p + Be reactions, a cut of the transverse e^+, e^- momenta $p_T \geq 0.175$ GeV/c has been taken in line with the experimental acceptance cut. For Pb + Au at 160 GeV/u (and semicentral collisions) the dominant yield for invariant masses 0.3 GeV $\leq M \leq 0.7$ GeV stems from $\pi^+\pi^-$ annihilation (cf. Fig. 5). Also in the Φ mass regime about 1 GeV there is a large contribution from K^+K^- and $\pi\rho$ annihilation to dileptons for both scenarios: with bare meson masses (upper part of Fig. 5) and with in-medium meson masses (lower part of Fig. 5). Whereas most of the processes (Dalitz and direct decays) occur in the vacuum at zero baryon density, the $\pi\pi \to \rho^0 \to e^+e^-$ and direct ρ^0 (from baryon-baryon and meson-baryon collisions) decay still occur at finite baryon density such that a dropping ρ mass also leads to a shift of the respective contribution to lower invariant masses M. In Fig. 5 both scenarios are compared to the preliminary data of the CERES collaboration [43]; due to the present statistics, however, there is no unique conclusion since the calculation with bare meson masses (upper part) also describes the data except for one point at 0.6 GeV (cf. also Ref. [23]). On the other hand, the present preliminary data match well with the calculation including the in-medium meson masses. We note that the comparison with the data in Fig. 5 has been performed for $b = 5$ fm, because for this impact parameter the charged particle multiplicity $dn_{ch}/d\eta \approx 260$ as for the experimental normalization (see below).

10

4.2 Dilepton yield versus charged particle multiplicity

The number of charged particles $dn_{ch}/d\eta$ in the pseudorapidity bin $2.1 \leq \eta \leq 3.1$ for Pb + Au at 160 GeV/u is shown in Fig. 6. The open circles are the result of our computations with 'free' meson masses, while the solid circles correspond to calculations when including the in-medium modifications of the meson masses. In both cases the charged particle multiplicity decreases with impact parameter practically linearly. For peripheral collisions there is no essential difference between both schemes as expected. For central collisions, however, the charged particle multiplicity in the 'dropping' meson mass scenario is slightly larger due to the reduction of the vector meson and antikaon production thresholds, which enhances the respective particle formation cross sections at high baryon density. Especially the subsequent decay of ρ and ω mesons to pions leads to a larger number of pions in the final expansion phase. We note, that due to the conservation of energy and momentum in each production event the enhanced number of vector mesons and antikaons at finite baryon density goes along with a lower number of those mesons, that do not change their quasiparticle properties in the medium (π, η, η' etc.).

Including the CERES acceptance cuts and mass resolution as described above, we show in Fig. 7 the dilepton yield integrated over the invariant mass range $0.3 \leq M \leq 1.0$ GeV,

$$\frac{dN/d\eta}{dn_{ch}/d\eta} = \int_{0.3~\mathrm{GeV}}^{1.0~\mathrm{GeV}} dM~\frac{dn_{e^+e^-}/(dMd\eta)}{dn_{ch}/d\eta} \qquad (27)$$

as a function of the charged particle multiplicity $dn_{ch}/d\eta$ without (open circles) and with (solid circles) in-medium mass modification. At small charged particle multiplicity, which corresponds to very peripheral collisions, the integrated dilepton yields coincide for both cases. With decreasing impact parameter the average baryon density and especially the pion density increases; as a consequence the contribution from pion annihilation to ρ^0 and subsequent decay to dileptons becomes larger. Since we gate on dileptons above the $\pi^+\pi^-$ annihilation threshold, also the integrated dilepton spectra increase with $dn_{ch}/d\eta$. Using 'free' meson masses we reach some plateau for low impact parameter which implies that the $\pi\pi$ annihilation contribution, divided by the pion density, becomes approximately constant. However, for the 'dropping' mass scenario the absolute dilepton yield above 0.3 GeV is smaller because the directly produced ρ-mesons (at high initial baryon density) also 'shine' in the invariant mass regime below 0.3 GeV (cf. lower part of Fig. 5). Furthermore, due to an initially higher vector meson density the initial pion density (due to energy conservation) is reduced as compared to the 'free' mass scenario and the corresponding pion annihilation contribution is also lowered to some extend. All effects together lead to an approximately linear increase of the integrated dilepton yield with the charged particle multiplicity in the 'dropping' mass picture. Experimental data with sufficient statistics should allow to disentangle the two schemes or disqualify the hadronic scenario as employed in the HSD transport approach.

5 Systematics of dilepton production from AGS to SPS energies

In this section we present a systematic analysis of various dilepton observables – the differential dilepton spectra, rapidity and transverse momentum distributions, the average transverse momentum – for p + Be and Pb + Pb collisions from AGS to SPS energies for the 'free' and 'dropping' mass scenarios.

5.1 Differential dilepton spectra

We first examine the differential dilepton spectra - integrated over rapidity and transverse momentum - with respect to their 'cocktail' decomposition. The respective spectra for p + Be at 10, 50, 450 GeV/u and for Pb + Pb at 10, 50, 160 GeV/u for $b = 2$ fm are shown in Figs. 8 – 10. For all cases we include a mass resolution of $\Delta M = 10$ MeV, which can be expected for future dilepton detector systems [44]. As seen from Figs. 8 – 10, there are no dramatic differences in the relative contribution of the various dilepton channels; the total yield (and especially the Φ decay) increase with bombarding energy quite smoothly. In case of central Pb + Pb collisions the dominance of the $\pi^+\pi^-$ annihilation component is most pronounced at 10 GeV/u in both scenarios and decreases with bombarding energy.

Since experimentally only the total spectra can be observed, we show in Fig. 11 the sum of all contributions for the 'free' (dashed lines) and 'dropping' mass scenario (solid lines) for central collisions of Pb + Pb at different bombarding energies to demonstrate the influence of in-medium effects for the mesons. For a mass resolution $\Delta M = 10$ MeV one can expect to observe not only the "usual" enhancement of the dilepton spectra by about a factor of 2 at invariant masses $0.3 \leq M \leq 0.6$ GeV, but also a sharp drop of the spectrum above the ω mass by a factor $4 - 6$ due to the shift of the ρ contribution to lower invariant masses. Furthermore, the peak from the ω meson becomes more pronounced since the 'background' from the ρ decay (either from πB, BB or $\pi\pi$ collisions) is significantly reduced. In the Φ mass region, furthermore, we find a small increase of the yield for the 'dropping' mass scheme at all energies from 10 – 160 GeV/u. Again, the relative modifications of the total spectrum are most pronounced at 10 GeV/u.

5.2 Transverse momentum distributions

In this subsection we explore if the transverse momentum distribution of the lepton pair might give some further criteria to distinguish between the different scenarios. In this respect the transverse momentum distributions – integrated over rapidity and the invariant mass $0.4 \leq M \leq 0.7$ GeV – are shown in Figs. 12 – 14 for p + Be at 10, 50, 450 GeV/u and for Pb + Pb at 10, 50, 160 GeV/u for $b = 2$ fm using $q_\perp$-bins of 50 MeV/c.

The main contribution in the invariant mass region $0.4 \leq M \leq 0.7$ GeV for p + Be comes from the η, ω Dalitz decays according to Fig. 8. The same decomposition can be observed in Fig. 12, where we display only the dominant channels. Performing

an exponential fit to the sum of all contributions (thick solid lines in Fig. 12) for $M \geq 0.4$ GeV the following slope parameters can be extracted from our calculations: 125 MeV at 10 GeV/u, 160 MeV at 50 GeV/u, and 185 MeV at 450 GeV/u.

Contrary to p + Be reactions, the dominant channels in the mass range $0.4 \leq M \leq 0.7$ GeV for central Pb + Pb collisions are the pion annihilation, ω Dalitz decay and direct decay of vector mesons. As shown before, including the in-medium 'dropping' masses we obtain a shift of the ρ meson contribution (cf. Figs. 9,10) to smaller invariant masses and one might expect same enhancement of the transverse momentum distribution at lower $q_\perp$ in this case. This effect is demonstrated in Fig. 13 where the transverse momentum spectra for the in-medium mass scheme (solid lines) are slightly softer than for the 'free' mass case (dashed lines). This tendency can also be seen from the slope parameters extracted for $q_T \geq 0.4$ GeV/c: 145 MeV at 10 GeV/u for the 'free' meson mass scheme – 130 MeV, when including the in-medium mass modification; at 50 GeV/u – 170 MeV and 155 MeV, respectively; at 160 GeV/u – 195 MeV and 180 MeV, respectively.

In order to clarify the origin of these differences, we present the channel decomposition for central Pb + Pb collisions at 160 GeV/u in Fig. 14 for both scenarios. The pion annihilation and ω Dalitz decay contribution, which are dominant in the invariant mass region considered, become slightly softer in the 'dropping' mass scenario. We note, however, that the transverse momentum spectra do not differ sizeably; according to the authors point of view they do not qualify very much for disentangling the different schemes.

5.3   Average transverse momentum $< q_T > (M)$

The dilepton average transverse momentum as a function of the invariant mass, $< q_T > (M)$, was already studied experimentally for hadron-hadron collisions a couple of years ago (cf. the reviews [45, 46]), where an increase of $< q_T >$ with M and bombarding energy was observed.

In our analysis the average transverse momentum for the channel k is defined as

$$< q_T >^k (M) = \frac{\sum_i w_i^k(q_{Ti}, M_i)\; q_{Ti}}{\sum_k \sum_i w_i^k(q_{Ti}, M_i)}, \tag{28}$$

where $w_i^k(q_{Ti}, M)$ is the probability of the individual dilepton event i (cf. Section 2.2). The total $< q_T >$ is the sum of the individual channels:

$$< q_T > (M) = \sum_k < q_T >^k (M). \tag{29}$$

The results of our computations are shown in Fig. 15 for p + Be at 10, 50 and 450 GeV including the contributions from the individual channels. Due to mass bins of 50 MeV the shapes from the vector mesons ω and Φ are not very pronounced. However, one can see the main tendency: the total $< q_T >$ increases with invariant mass and bombarding energy in the same way as for hadron-hadron collisions [45, 46].

A similar behaviour of the average transverse momentum is found for central collisions of Pb + Pb at 10, 50 and 160 GeV/u in Fig. 16, were we have plotted the total $< q_T >$ for both scenarios, i.e. without (dashed lines) and with (solid lines) 'dropping' of meson masses. The channel decomposition is shown only for the 'free' mass scenario. Contrary to p + Be the contribution from $\pi^+\pi^-$ annihilation dominates from 0.5 – 0.8 GeV at all bombarding energies, however, we do not find a pronounced difference in the total $< q_T >$ between both mass schemes.

5.4 Rapidity distribution of lepton pairs

The results of our calculations for the dilepton rapidity distribution in the nucleon-nucleon center-of-mass system are displayed in Figs. 17,18. In analogy to the previous cases we study the systems p + Be at 10, 50, 450 GeV/u and Pb + Pb at 10, 50, 160 GeV/u ($b = 2$ fm) integrating over the transverse momentum and the invariant mass range $0.4 \leq M \leq 0.7$ GeV. As seen from Figs. 17,18 the shapes of the rapidity distributions are quite similar. An enhancement of about a factor $1.5 - 2$ for Pb + Pb can be seen at midrapidity when employing in-medium meson masses (solid lines), while there is practically no difference at more forward or backward rapidities. Again this enhancement is most pronounced at 10 GeV/u for Pb + Pb and decreases with bombarding energy as expected from Fig. 1.

6 Direct photons

Directly radiated thermal photons have been considered as an independent probe to study the hot and dense nuclear matter produced in ultrarelativistic nucleus-nucleus collisions [47, 48]. However, an experimental measurement of direct photons is a quite complicated task due to the background from hadronic decays. Only recently first upper limits for direct photon spectra have been reported by the WA80 collaboration [49] for S + Au at 200 GeV/u. In the latter study photons from π^0 and η Dalitz decays have been subtracted from the total photon signal; their spectra thus can be interpreted as upper bounds for the direct photon cross section.

A first calculation of the direct photon radiation from a quark-gluon-plasma (QGP) was performed a couple of years ago in Ref. [50]; various hydrodynamical model calculations followed (cf. [49, 51] and references therein), where the radiation from a QGP [52] has been compared to the radiation from a pure hadron gas scenario [53]. The comparison of the various models with the WA80 data [49], however, has demonstrated only the inapplicability of hadronic thermal models with high initial temperature. In this respect it should be quite useful to compare the WA80 upper limits with the results of a nonthermal model – such as the HSD transport approach – to find out possible conflicts with the hadronic scenario employed.

6.1 Description of elementary channels

In our analysis we take into account the following processes for photon production: $a_1 \to \pi\gamma$, $\omega \to \pi\gamma$, $\eta' \to \rho\gamma$ or $\omega\gamma$. The π^0 and η decays are already subtracted

experimentally and thus don't have to be taken into account in our calculations.

The treatment of photon production in the HSD approach is quite similar to that for dileptons, however, using the branching ratios:

$$\frac{\Gamma_{a_1 \to \pi\gamma}}{\Gamma_{a_1}} \simeq 1.6 \times 10^{-3}, \quad \frac{\Gamma_{\omega \to \pi\gamma}}{\Gamma_\omega} = 0.085, \quad \frac{\Gamma_{\eta' \to \rho\gamma}}{\Gamma_{\eta'}} = 0.3, \quad \frac{\Gamma_{\eta' \to \omega\gamma}}{\Gamma_{\eta'}} = 0.03. \qquad (30)$$

We discard baryon-baryon, meson-baryon and meson-meson bremsstrahlung in our present study since these channels were found to be of minor importance for dilepton production in case of S + Au at 200 GeV/u in Ref. [20]. Furthermore, the soft-photon approximation employed in [20] is questionable at these energies according to the studies in Refs. [54, 55].

6.2   Comparison with experimental data for S + Au

In Fig. 19 we show the result of our calculations for photon production in central S + Au collisions at 200 GeV/u in comparison with the experimental data [49]. The computations were performed at $b = 2$ fm including the experimental rapidity cut $2.1 \leq y \leq 2.9$. As seen form Fig. 19 the main contribution in our calculation comes from $\eta' \to \rho/\omega \, \gamma$ decays at low $q_T \leq 0.4$ GeV and from $\omega \to \pi\gamma$ for $q_T \geq 0.4$; the solid line is the sum of all contributions which is still well below the upper limits of WA80.

For the process $a_1 \to \pi\gamma$ we explore again both scenarios, i.e. without (dashed line) and with (dashed-dotted line) in-medium mass modification. In fact, the dropping of the a_1 mass leads to a sizeable enhancement of a_1 mesons in the reaction zone and thus to a significant enhancement of the photon spectra from the a_1 as pointed out in Refs. [39, 51]. However, the relative contribution from the a_1 decay is still far below the 'background' from η' and ω decays. Thus, even in case of the 'dropping' meson masses we do not get in any conflict with the upper limits imposed by the WA80 data [49].

7   Summary

In this work we have studied dilepton production in proton and heavy-ion induced reactions from 10 – 450 GeV or 10 – 160 GeV/u, respectively, on the basis of the covariant transport approach HSD [4]. We have incorporated the contributions of the Dalitz-decay of the η, ω, η', a_1 as well as $\pi^+\pi^-$ annihilation and the direct dilepton decay of the vector mesons ρ, ω, Φ as well as K^+K^- and $\pi\rho$ channels. It is found that for p + Be at 450 GeV the mesonic decays almost completely determine the dilepton yield, whereas in Pb + Au reactions the $\pi^+\pi^-, K^+K^-$ annihilation channels and $\pi\rho$ collisions contribute substantially. The experimental data taken by the CERES collaboration [11, 43] generally are underestimated by the calculations for invariant masses 0.35 GeV $\leq M \leq$ 0.65 GeV when using 'free' form factors for the pion and ρ-meson in line with Refs. [19, 21, 29].

We have, furthermore, examined the effects of 'dropping' ρ, ω, Φ, K^- and a_1 masses on the dilepton spectra, which generally leads to an improvement in the description of

the experimental data from the CERES [11, 43] and HELIOS-3 collaborations (cf. also Refs. [19, 20, 28, 29]). In order to allow for a clearer distinction between the different scanarios we have performed systematic studies for p + Be and central Pb + Pb collisions from 10 – 450 or 160 GeV/u, respectively, with respect to the transverse momentum distribution of the dilepton pair and their rapidity distribution. At all bombarding energies the in-medium effects are most pronounced at midrapidity, but the modifications in the transverse momentum spectra are only very moderate, such that the $q_\perp$ distributions do not qualify very much for quantifying the in-medium effects. The same holds for the average transverse momentum of the dilepton pair as a function of the invariant mass M. A more pronounced variation is obtained for the dilepton yield (integrated for $M \geq 0.3$ GeV) as a function of the charged particle multiplicity at midrapidity (cf. Fig. 7), where the 'free' and 'dropping' meson mass scenarios differ significantly. This sensitivity should be explored in the next round of experiments at the SPS.

Apart from the enhancement of the e^+e^- yield for invariant masses $0.3 \leq M \leq 0.7$ GeV in case of 'dropping' meson masses, one should also see a decrease by factors $4 – 6$ in the latter scheme for $0.8 \leq M \leq 1$ GeV in case of central Pb + Pb collisions (cf. Fig. 11), provided that the experimental mass resolution is in the order of about 10 MeV. The relative differences between the 'free' and 'dropping' mass schemes become larger when decreasing the bombarding energy from 160 GeV/u to 50 GeV/u and even to 10 GeV/u. According to Fig. 1 there might be a maximum sensitivity around 20 – 30 GeV/u, however, the relative change of the dilepton spectrum from 10 – 50 GeV/u – apart from an overall increase by about a factor of 3 – is not very pronounced.

We have, furthermore, explored if the hadronic reactions rates from the HSD transport approach might come in conflict with the upper limits for the direct photon spectrum in central collisions of S + Au from the WA80 collaboration [49], because the photon multiplicity from a_1 decay might be dramatically enhanced in a phase with a partial restoration of chiral symmetry as suggested in Ref. [51]. Our computations, however, including also the processes $\eta' \to \rho/\omega\,\gamma; \omega \to \pi\gamma$ do not show any indications for this, since the sum-spectra are still below the upper limits from WA80 by at least a factor of 3. In this respect we do not find any inconsistencies within the hadronic picture of the nucleus-nucleus collision. As pointed out in Ref. [56], there might be problems due to the large energy densities reached in central Pb + Pb collisions (above 3 GeV/fm^3) at 160 GeV/u, where one generally believes that droplets of a quark-gluon-plasma (QGP) should be formed.

We finally note, that apart from the multi-differential dilepton spectra – investigated in this work – also dilepton angular anisotropies should provide additional information for disentangling the production channels experimentally. As analyzed in Ref. [33] this additional observable, however, requires a large acceptance in the dilepton spectrometer, which is presently not fulfilled for the existing setups, but should be addressed in experiments with HADES.

Acknowledgments

References

[1] G. Brown and M. Rho, Phys. Rev. Lett. 66 (1991) 2720.

[2] M. C. Birse, J. Phys. G20 (1994) 1537.

[3] T. Abbot et al., Nucl. Phys. A544 (1992) 237.

[4] W. Ehehalt and W. Cassing, Nucl. Phys. A602 (1996) 449.

[5] B. Braun-Munzinger, J. Stachel, J. P. Wessels, and N. Xu, Phys. Lett. B344 (1995) 43.

[6] G. Q. Li, C. M. Ko, and X. S. Fang, Phys. Lett. B329 (1994) 149.

[7] W. Cassing, E. L. Bratkovskaya, U. Mosel, S. Teis, and A. Sibirtsev, Nucl. Phys. A614 (1997) 415.

[8] G. Roche et al., Phys. Rev. Lett. 61 (1988) 1069.

[9] C. Naudet et al., Phys. Rev. Lett. 62 (1989) 2652.

[10] G. Roche et al., Phys. Lett. B226 (1989) 228.

[11] G. Agakichiev et al., Phys. Rev. Lett. 75 (1995) 1272.

[12] M. A. Mazzoni, Nucl. Phys. A566 (1994) 95c; M. Masera, Nucl. Phys. A590 (1995) 93c.

[13] T. Åkesson et al., Z. Phys. C68 (1995) 47.

[14] C. Baglin et al., NA38, Phys. Lett. B220 (1989) 471; B251 (1990) 465.

[15] M. Gonin et al., Nucl. Phys. A610 (1996) 404c.

[16] Gy. Wolf, G. Batko, W. Cassing, U. Mosel, K. Niita, and M. Schäfer, Nucl. Phys. A517 (1990) 615;

[17] L. Xiong, Z. G. Wu, C. M. Ko, and J. Q. Wu, Nucl. Phys. A512 (1990) 772.

[18] P. Koch, Phys. Lett. B288 (1992) 187; B. Kämpfer, P. Koch, and O. P. Pavlenko, Phys. Rev. C49 (1994) 1132.

[19] G. Q. Li, C. M. Ko, and G. E. Brown, Phys. Rev. Lett. 75 (1995) 4007.

[20] W. Cassing, W. Ehehalt, and C. M. Ko, Phys. Lett. B363 (1995) 35.

[21] V. Koch and C. Song, Phys. Rev. C54 (1996) 1903.

[22] D. K. Srivastava, B. Sinha, and C. Gale, Phys. Rev. C53 (1996) R567.

[23] L. A. Winckelmann, C. Ernst, L. Gerland, J. Konopka, S. Soff et al., nucl-th/9610042.

[24] M. Herrmann, B. Friman, and W. Nörenberg, Nucl. Phys. A560 (1993) 411.

[25] M. Asakawa, C. M. Ko, P. Lévai, and X. J. Qiu, Phys. Rev. C46 (1992) R1159.

[26] G. Chanfray and P. Schuck, Nucl. Phys. A545 (1992) 271c.

[27] R. Rapp, G. Chanfray, and J. Wambach, Phys. Rev. Lett. 76 (1996) 368.

[28] W. Cassing, W. Ehehalt, and I. Kralik, Phys. Lett. B377 (1996) 5.

[29] C. M. Ko, G. Q. Li, G. E. Brown, and H. Sorge, Nucl. Phys. A610 (1996) 342c.

[30] K. Weber, B. Blättel, W. Cassing, H.-C. Dönges, V. Koch, A. Lang, and U. Mosel, Nucl. Phys. A539 (1992) 713.

[31] D. B. Kaplan and A. E. Nelson, Phys. Lett. B175 (1986) 57.

[32] T. Hatsuda and S. Lee, Phys. Rev. C46 (1992) R34.

[33] E. L. Bratkovskaya, W. Cassing, and U. Mosel, nucl-th/9609050; Z. Phys. C, in print.

[34] Gy. Wolf, W. Cassing, W. Ehehalt, and U. Mosel, Prog. Part. Nucl. Phys. 30 (1993) 273.

[35] Gy. Wolf, W. Cassing, and U. Mosel, Nucl. Phys. A552 (1993) 549.

[36] C. Gale and J. Kapusta, Phys. Rev., C35 (1987) 2107.

[37] G. Q. Li and C. M. Ko, Nucl. Phys. A582 (1995) 731.

[38] L. G. Landsberg, Phys. Rep. 128 (1985) 301.

[39] L. Xiong, E. Shuryak, and G. E. Brown, Phys. Rev. D46 (1992) 3789.

[40] C. M. Ko, Phys. Rev. C23 (1981) 2760.

[41] H. Appelshäuser et al., GSI Annual Report, 1995, p. 54.

[42] E. L. Bratkovskaya, W. Cassing, and U. Mosel, Phys. Lett. B367 (1996) 12.

[43] Th. Ullrich et al., Nucl. Phys. A610 (1996) 317c; A. Drees, Nucl. Phys. A610 (1996) 536c.

[44] J. Stachel, private communication.

[45] N. S. Craigie, Phys. Rep. 47 (1978) 2.

[46] R. Stroynowski, Phys. Rep. 71 (1980) 2.

[47] P. V. Ruuskanen, Nucl. Phys. A544 (1992) 169c.

[48] J. Kapusta, Nucl. Phys. A566 (1994) 45c.

[49] R. Albrecht et al., Phys. Rev. Lett. 76 (1996) 3506.

[50] E. Shuryak, Phys. Lett. B78 (1978) 150; Sov. J. Nucl. Phys. 28 (1978) 408.

[51] C. M. Hung and E. V. Shuryak, hep-ph/9608299.

[52] D. K. Srivastava and B. Sinha, Phys. Rev. Lett. 73 (1994) 316.

[53] A. Dumitru, U. Katscher, J. A. Maruhn, H. Stöcker, W. Greiner, and D. H. Rischke, Phys. Rev. C51 (1995) 2166.

[54] P. Lichard, Phys. Rev. D51 (1995) 6017.

[55] H.C. Eggers, C. Gale, R. Tabti, K. Haglin, hep-ph/9604372.

[56] W. Cassing and C. M. Ko, nucl-th/9609025, Phys. Lett. B, in print.
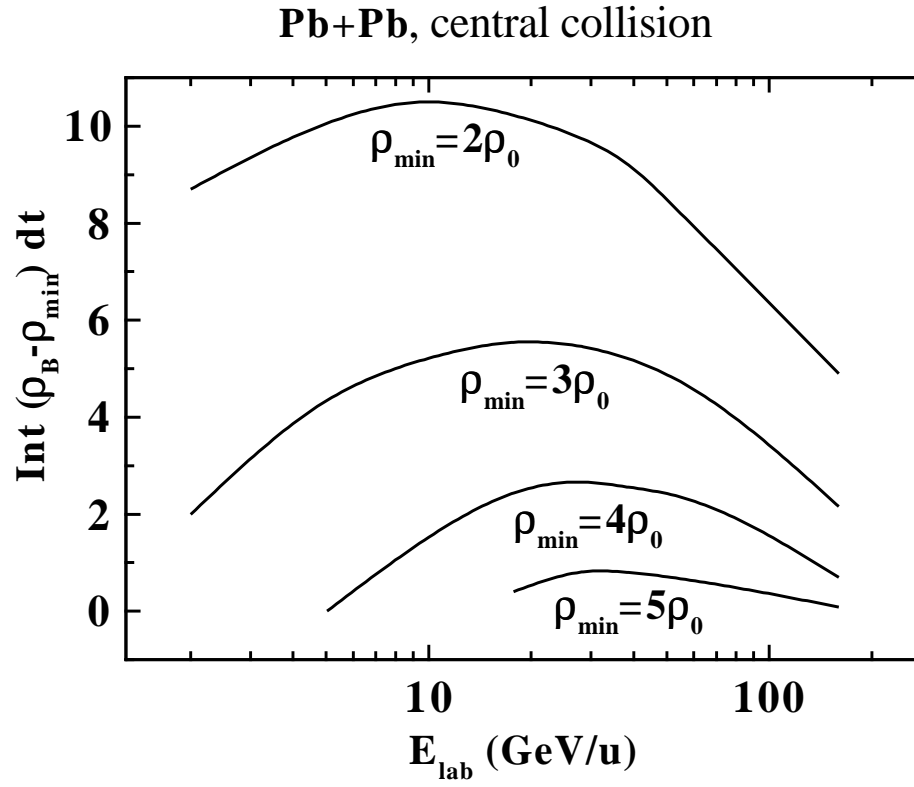
Figure 1: The quantity F (Eq. (25)) for central Pb + Pb collisions as a function of the bombarding energy per nucleon for 4 different cuts in ρ_{min}.
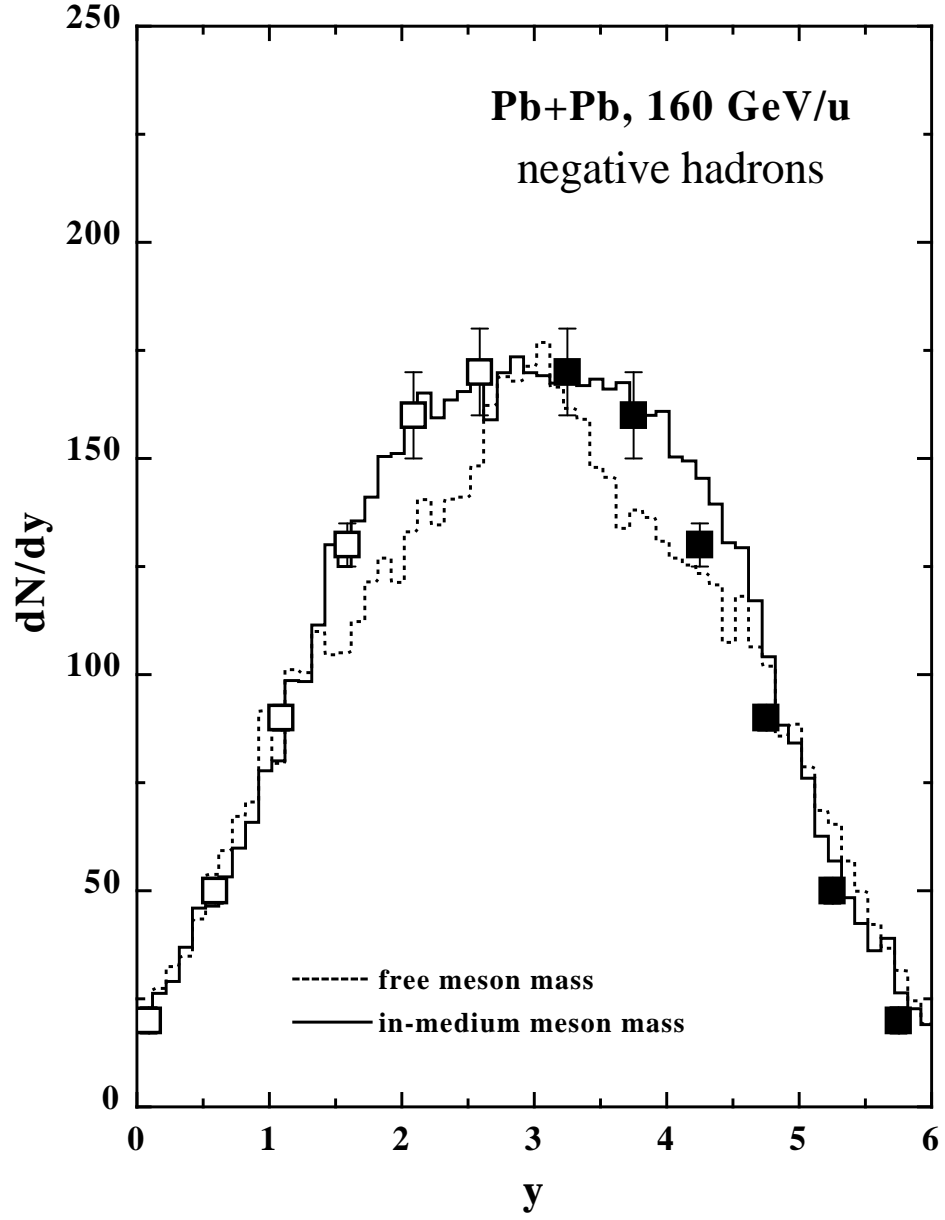
Figure 2: The preliminary rapidity distribution of negative hadrons from NA49 [41] (full squares) in comparison to the HSD results. The solid line corresponds to a calculation (at $b = 2$ fm) including the 'dropping' meson masses from Eqs. (5), (6), whereas the dotted line results from a calculation with bare meson masses. The open squares are obtained by reflecting the full squares at midrapidity.
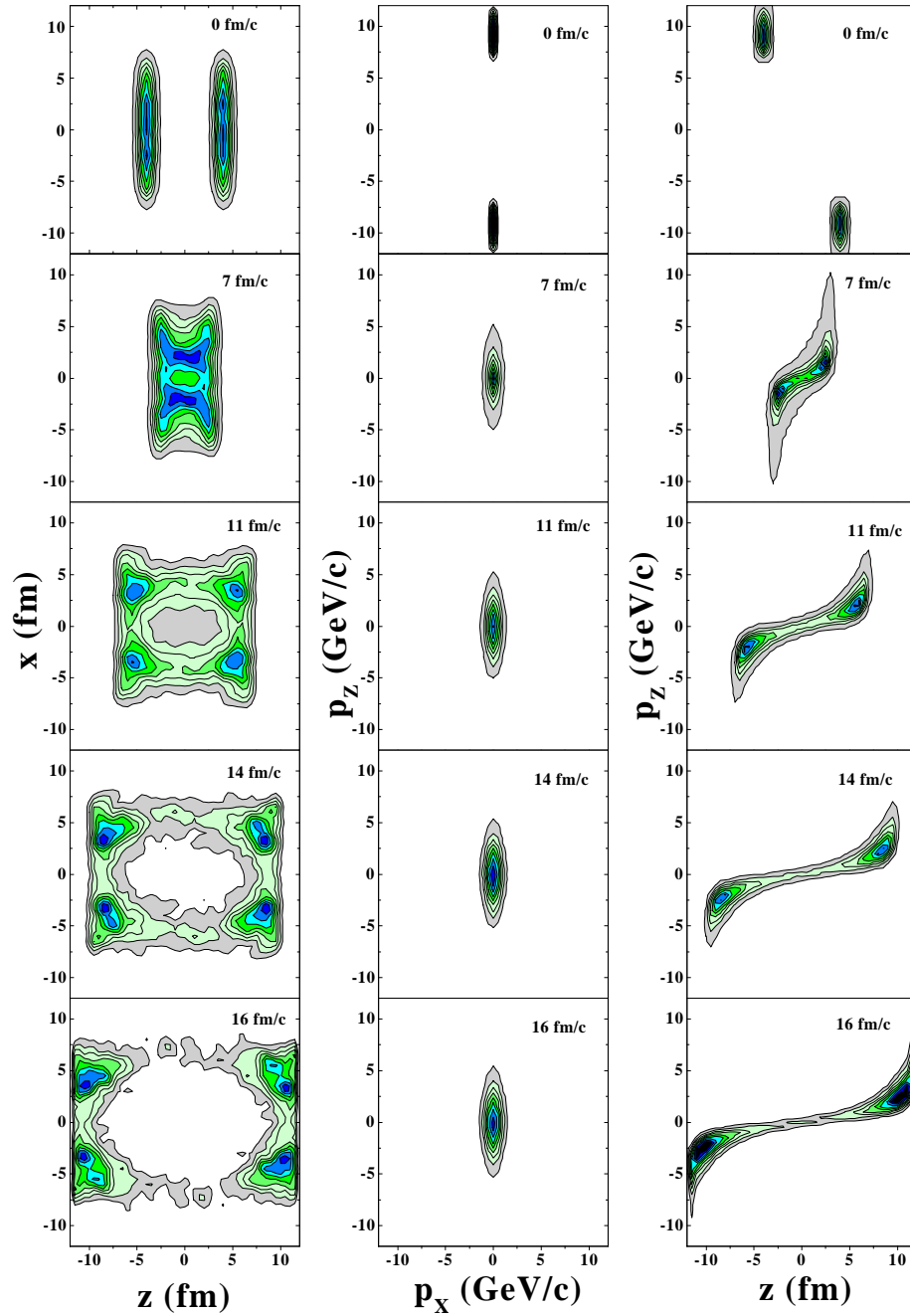
Figure 3: Baryon density distribution (left column), momentum space (middle column) and phase-space distribution (right column) for a 160 GeV/u Pb + Pb collision at $b = 0$ fm for various times in fm/c.
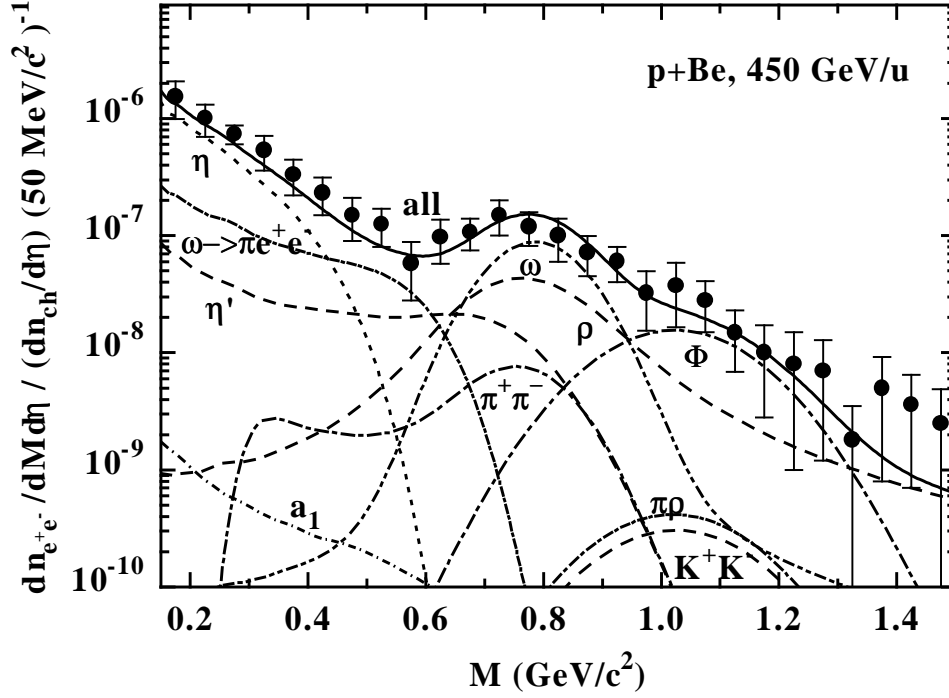
Figure 4: The calculated dilepton spectra (full solid line) for p + Be at 450 GeV/u in comparison with the data from Ref. [11]. The thin lines indicate the individual contributions from the different production channels including the CERES-acceptance and mass resolution; i.e. starting at low M: $\eta \to \gamma e^+ e^-$ (dashed line), $\omega \to \pi^0 e^+ e^-$ (dot-dashed line), $\eta' \to \gamma e^+ e^-$ (long dashed line), $a_1 \to \pi e^+ e^-$ (dot-dashed line); for $M \approx 0.8$ GeV: $\omega \to e^+ e^-$ (dot-dot-dashed line), $\rho^0 \to e^+ e^-$ (dashed line), $\pi^+ \pi^- \to e^+ e^-$ (dot-dashed line); for $M \approx 1$ GeV: $\Phi \to e^+ e^-$ (dot-dashed line), $\pi\rho \to e^+ e^-$ (dot-long dashed line), $K\bar{K} \to e^+ e^-$ (dashed line).

24
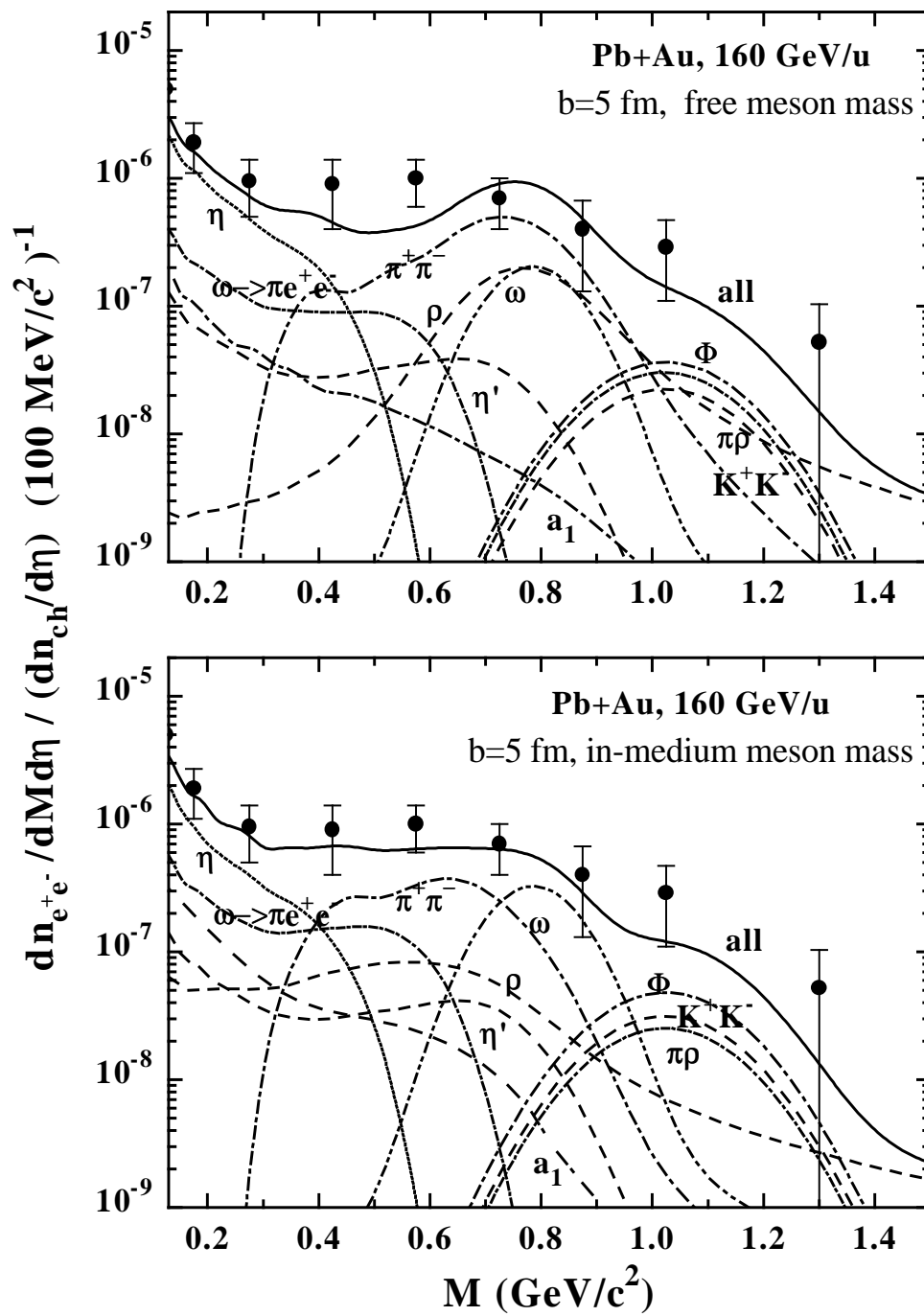
Figure 5: Dilepton invariant mass spectra for semicentral collisions of Pb + Au at 160 GeV/u (full solid lines) in comparison to the preliminary data of the CERES collaboration [43]. The upper part shows the results of a calculation with bare meson masses whereas the lower part includes the 'dropping' meson masses (Eqs. (5),(6)). The assignment of the individual contributions is the same as in Fig. 4.
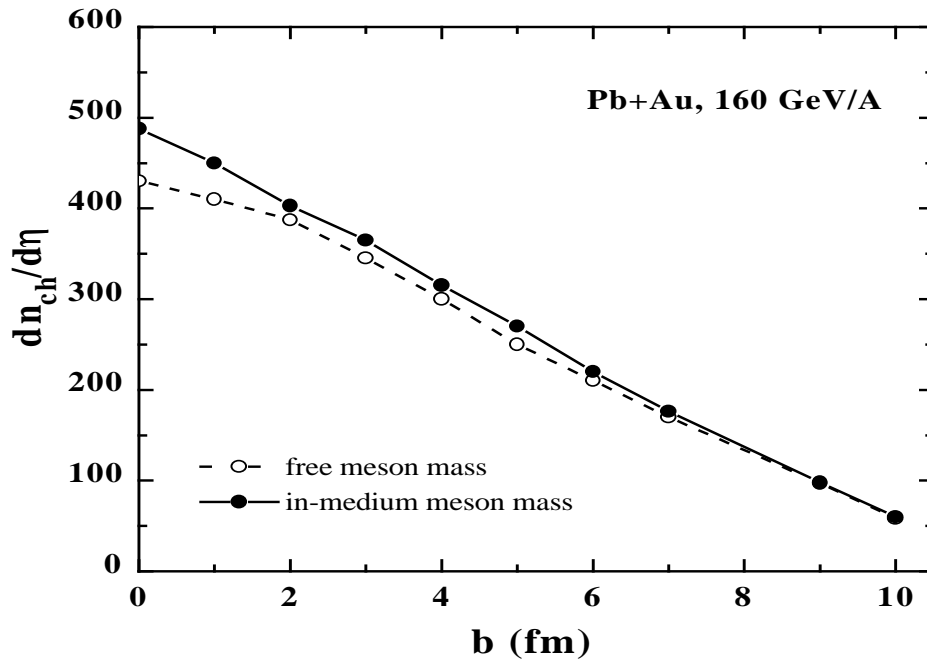
Figure 6: The charged particle multiplicity $dn_{ch}/d\eta$ for Pb + Au at 160 GeV/u as a function of the impact parameter b for the free meson mass scheme (dashed line) and the dropping meson mass scenario (solid line).
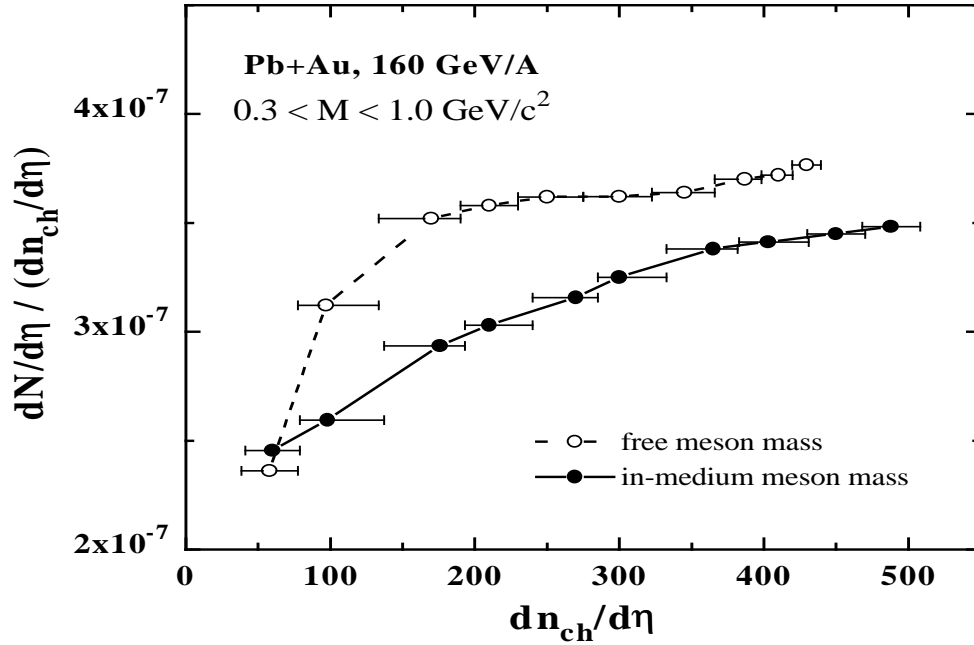
Figure 7: The differential dilepton spectra for Pb + Au at 160 GeV/u integrated over the invariant mass region $0.3 \leq M \leq 1.0$ GeV as a function of the charged particle multiplicity $dn_{ch}/d\eta$ without (open circles) and with (solid circles) the in-medium mass modification of the mesons.
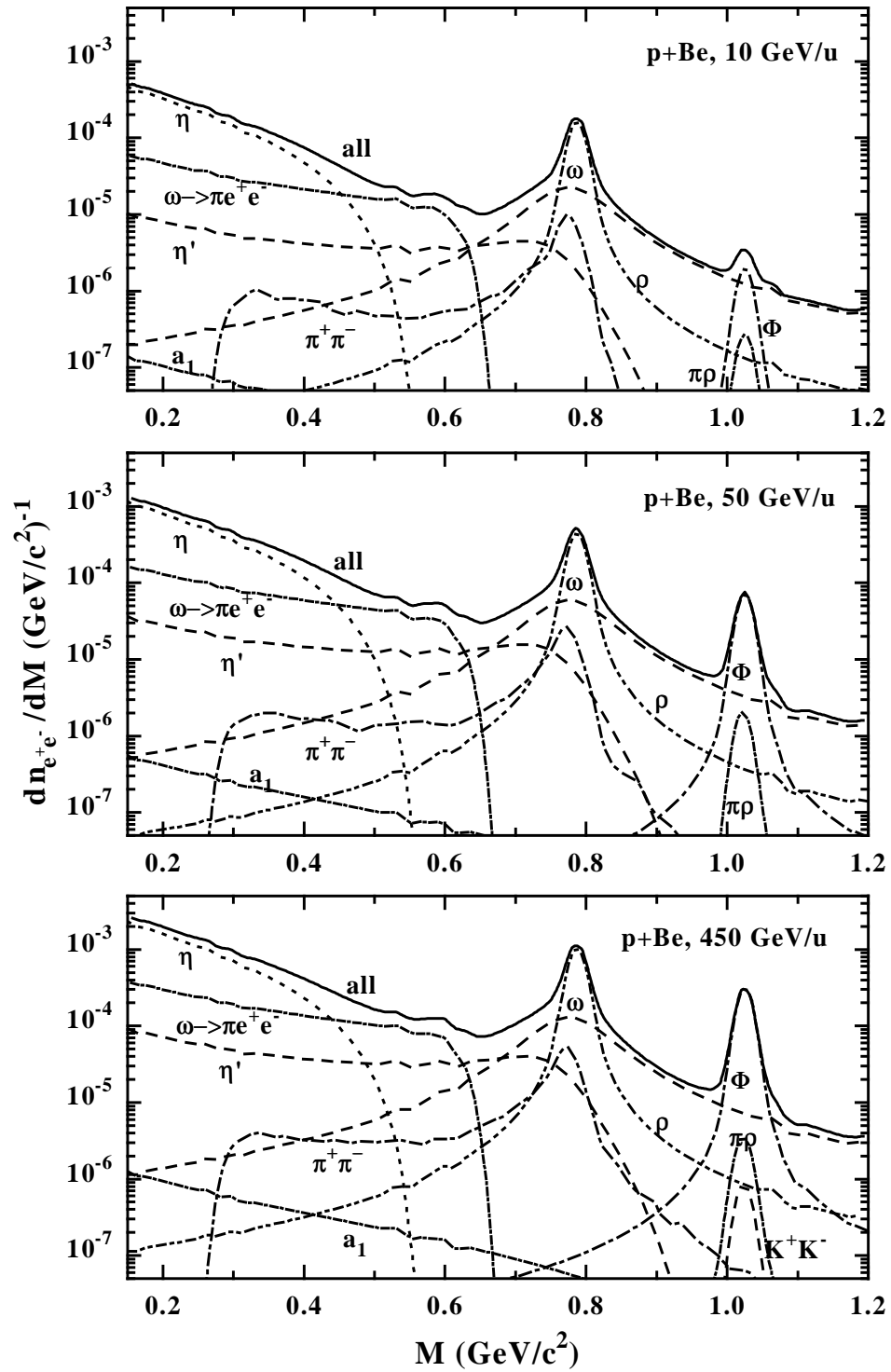
Figure 8: The differential dilepton spectra for p + Be at 10, 50, and 450 GeV. The thick solid lines display the sum of all channels whereas the individual contributions are given in terms of the thinner lines. The assignment of the individual contributions is the same as in Fig. 4. The mass resolution employed is $\Delta M = 10$ MeV.
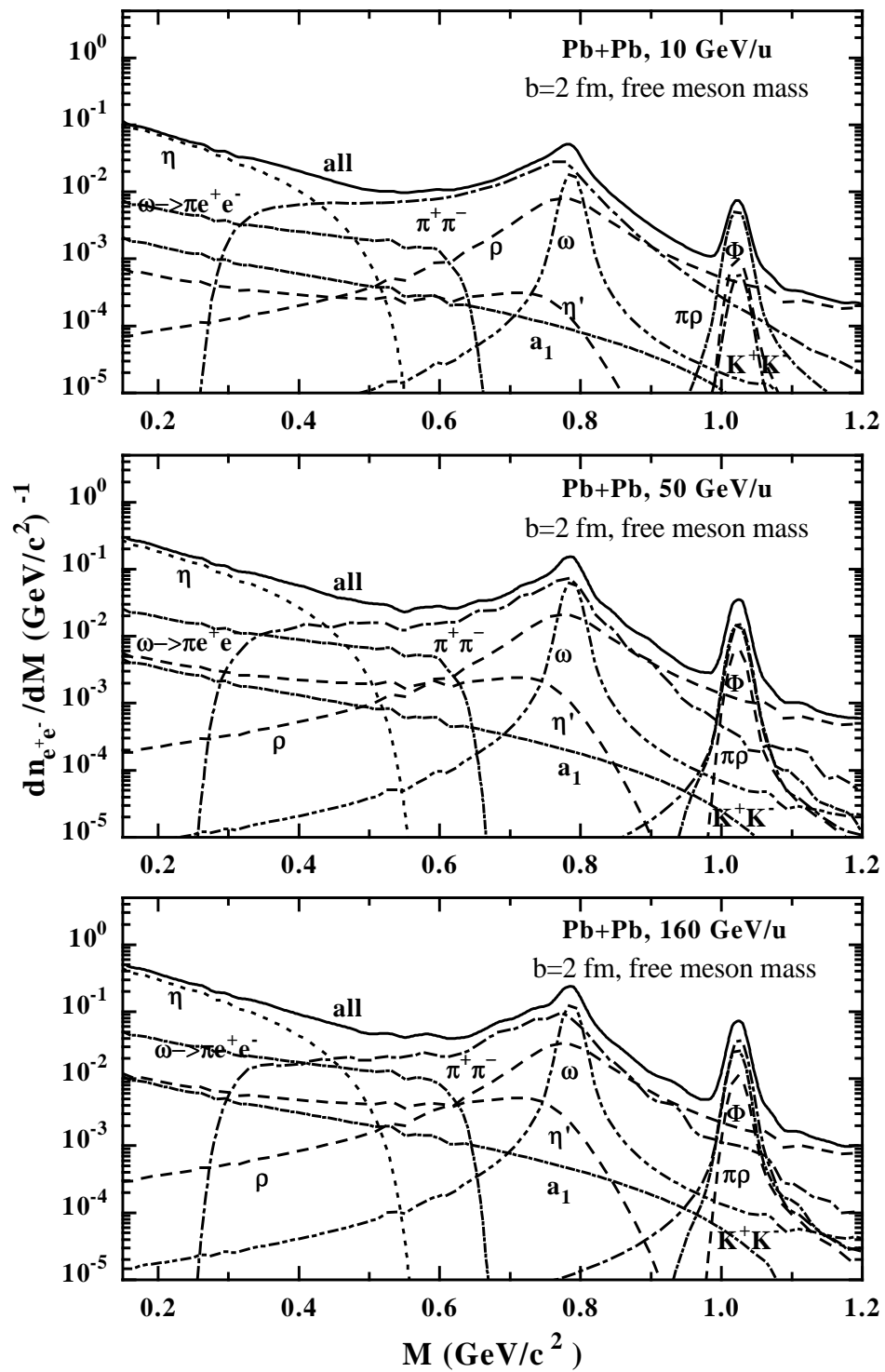
Figure 9: The differential dilepton spectra for Pb + Pb at 10, 50, 160 GeV/u at $b = 2$ fm within the 'free' meson mass scenario. The assignment of the individual contributions is the same as in Fig. 4. The mass resolution employed is $\Delta M = 10$ MeV.
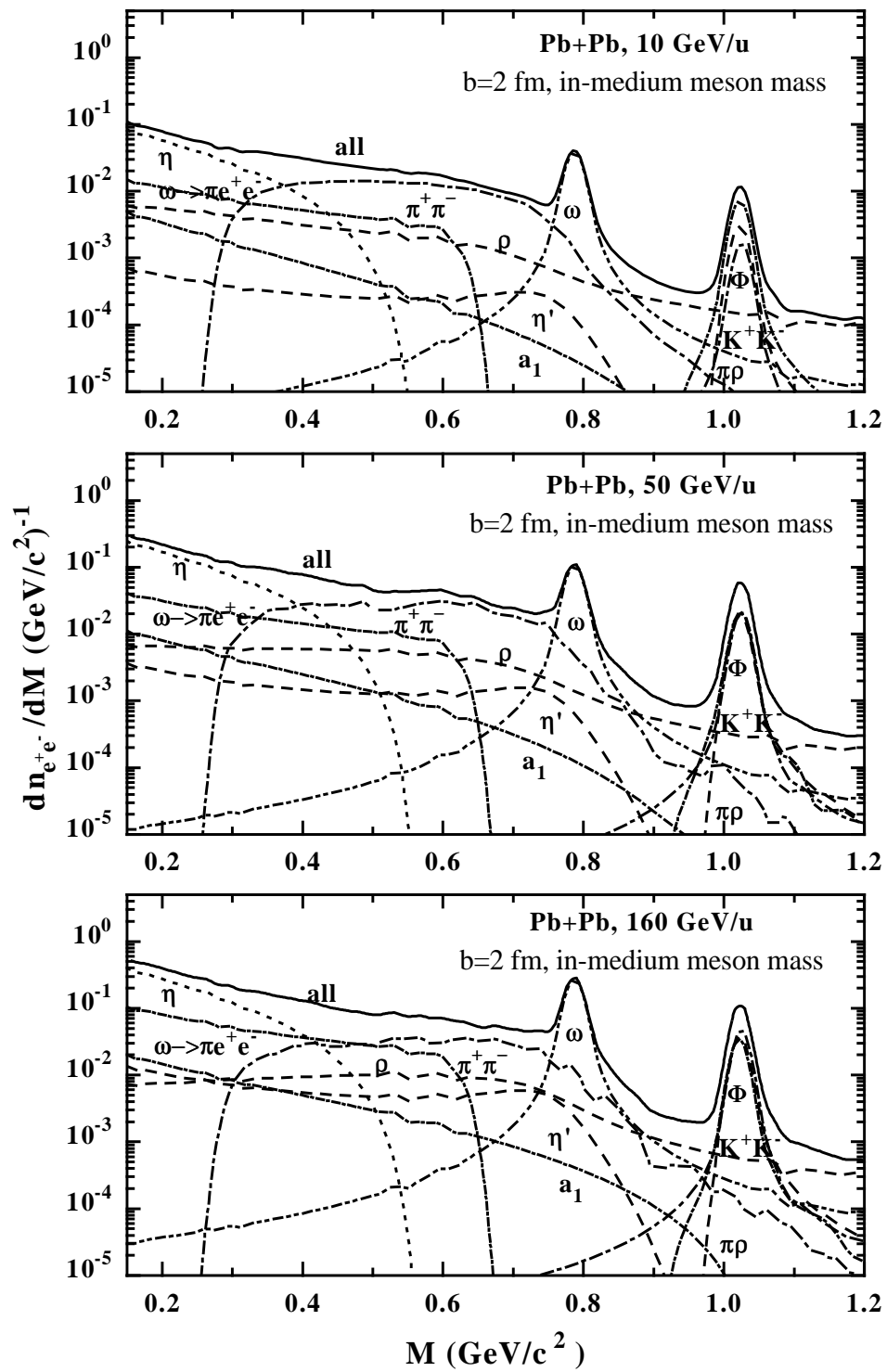
Figure 10: The differential dilepton spectra for Pb + Pb at 10, 50, 160 GeV/u at $b = 2$ fm within the in-medium meson mass scenario. The assignment of the individual contributions is the same as in Fig. 4. The mass resolution employed is $\Delta M = 10$ MeV.
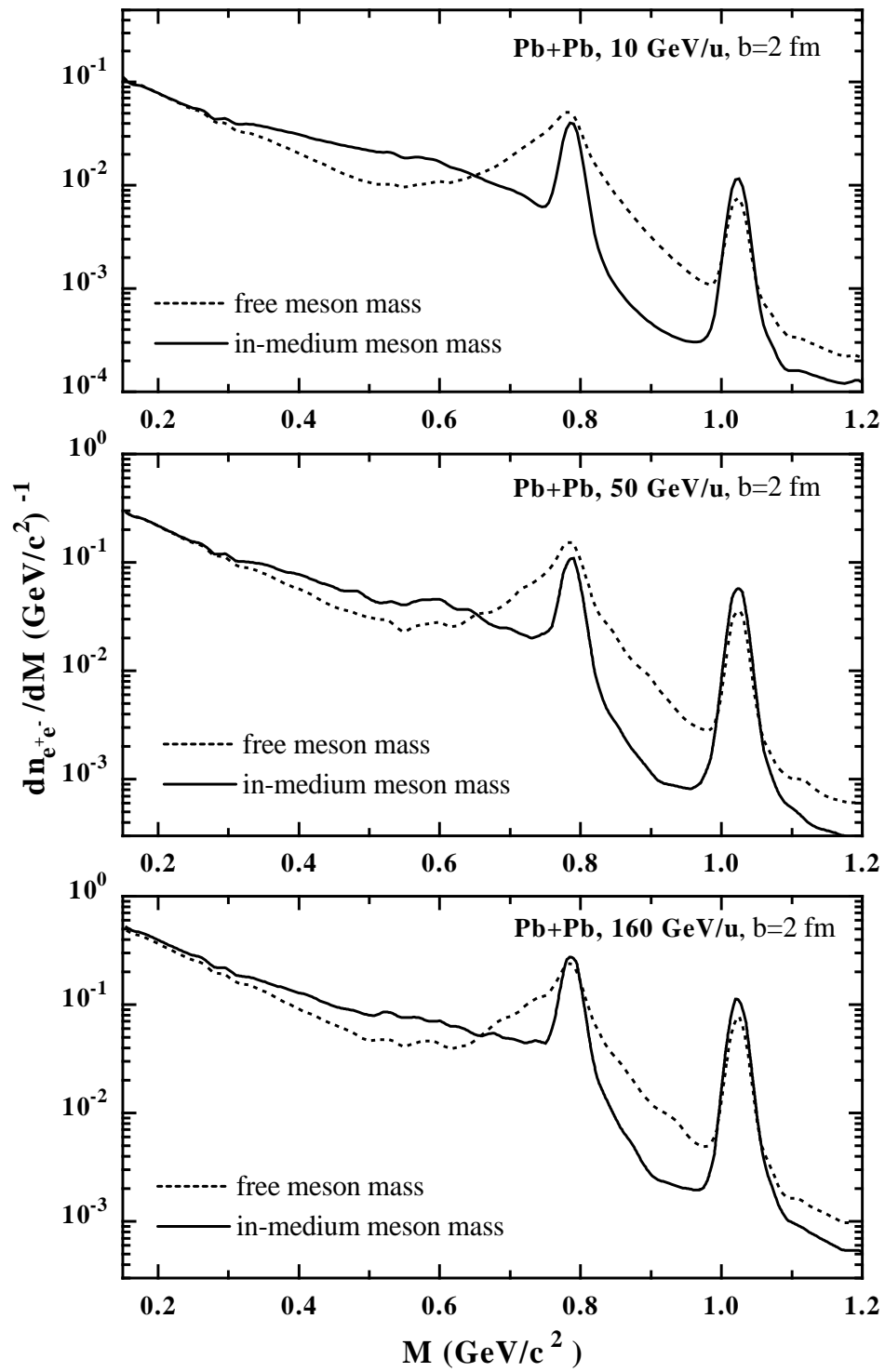
Figure 11: The differential dilepton spectra for Pb + Pb at 10, 50, 160 GeV/u at $b = 2$ fm without (dashed lines) and with in-medium meson mass modification (solid lines) for a mass resolution $\Delta M = 10$ MeV.
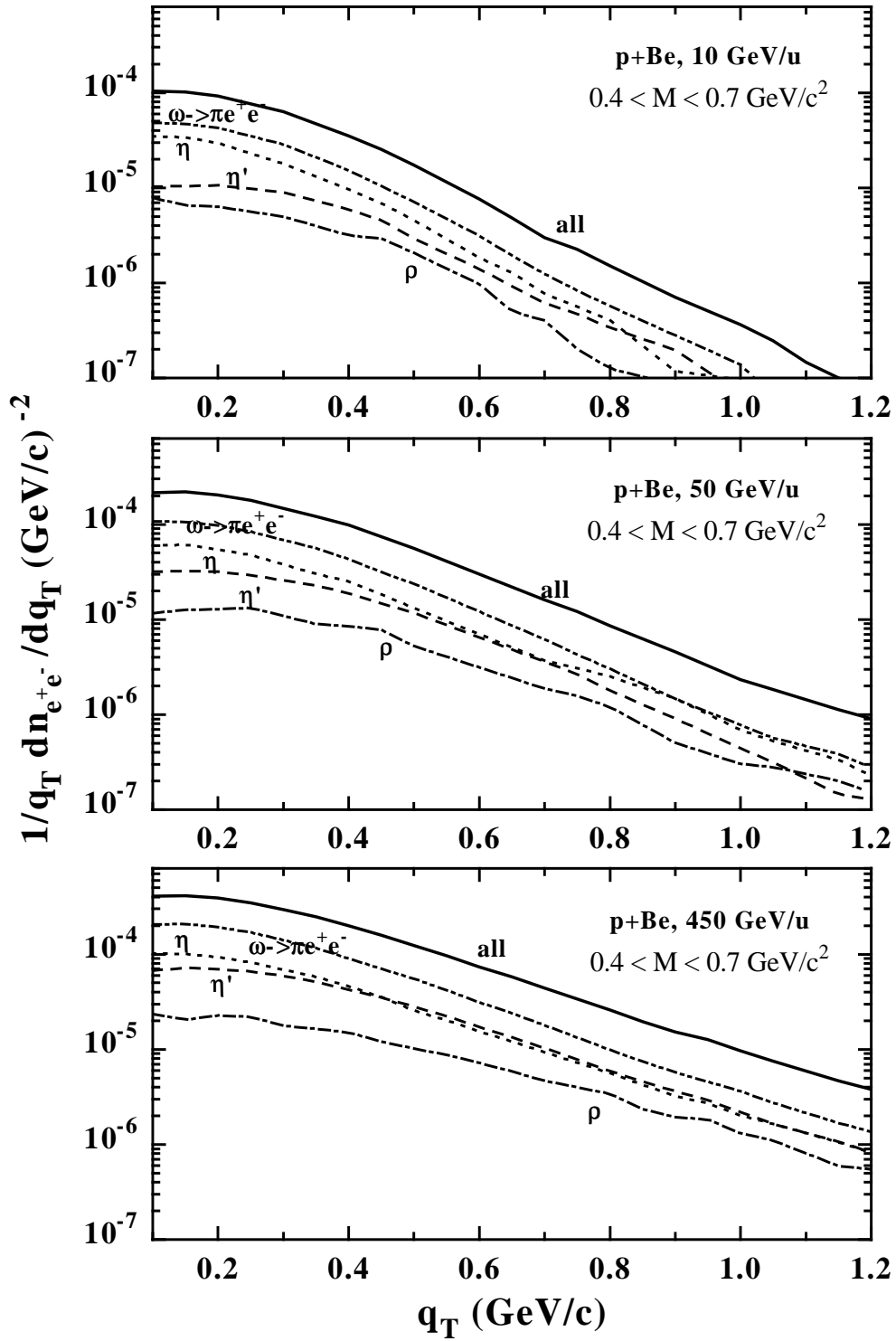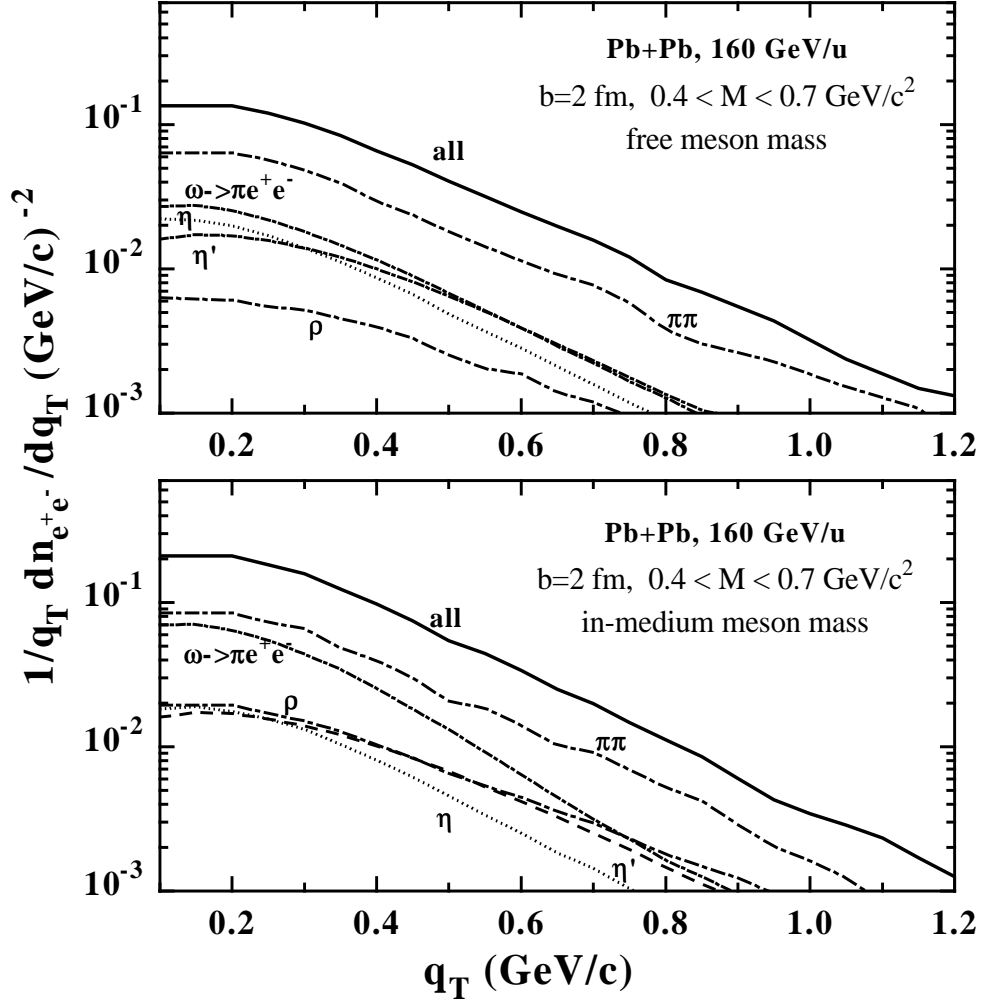
Figure 12: The channel decomposition for the average transverse momentum distribution in the invariant mass range $0.4 \leq M \leq 0.7$ GeV for p + Be at 10, 50, and 450 GeV; all contributions (solid line), $\omega \to \pi^0 e^+ e^-$ (dot-dot-dashed line), $\eta \to \gamma e^+ e^-$ (short dashed line), $\eta' \to \gamma e^+ e^-$ (long dashed line), $\rho^0 \to e^+ e^-$ (dot-dashed line).

31
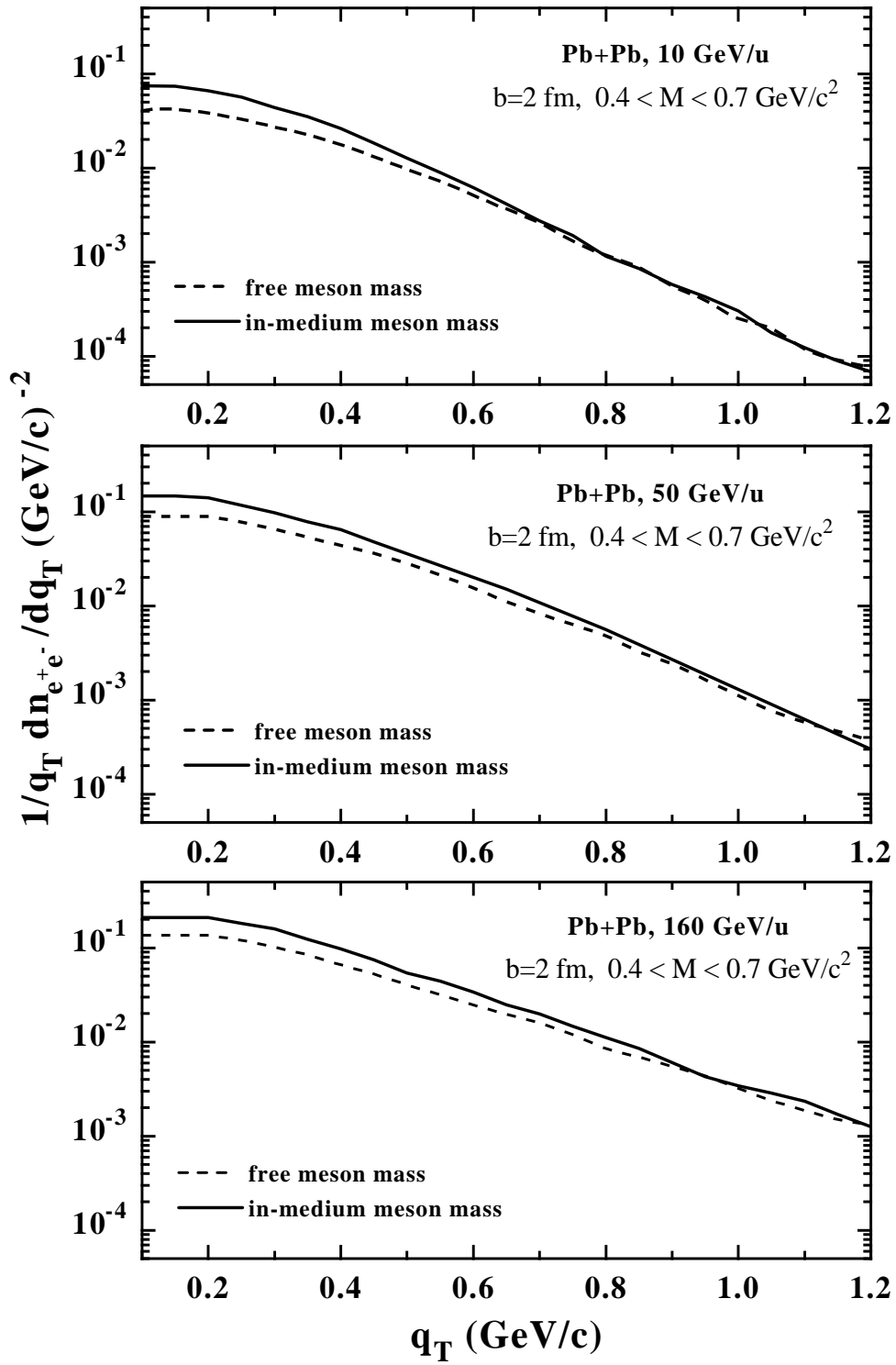
Figure 13: The transverse momentum distribution for the invariant mass range $0.4 \leq M \leq 0.7$ GeV for Pb + Pb at 10, 50, and 160 GeV/u at $b = 2$ fm without (dashed lines) and with in-medium meson mass modification (solid lines).

Figure 14: The channel decomposition for the transverse momentum distribution for the invariant mass range $0.4 \leq M \leq 0.7$ GeV for Pb + Pb at 160 GeV/u at $b = 2$ fm without (upper part) and with in-medium meson mass modification (lower part); all contributions (solid line), $\pi^+\pi^- \rightarrow e^+e^-$ (upper dot-dashed line), $\omega \rightarrow \pi^0 e^+e^-$ (short dot-dashed line), $\eta \rightarrow \gamma e^+e^-$ (dotted line), $\eta' \rightarrow \gamma e^+e^-$ (dashed line), $\rho^0 \rightarrow e^+e^-$ (lower dot-dashed line).
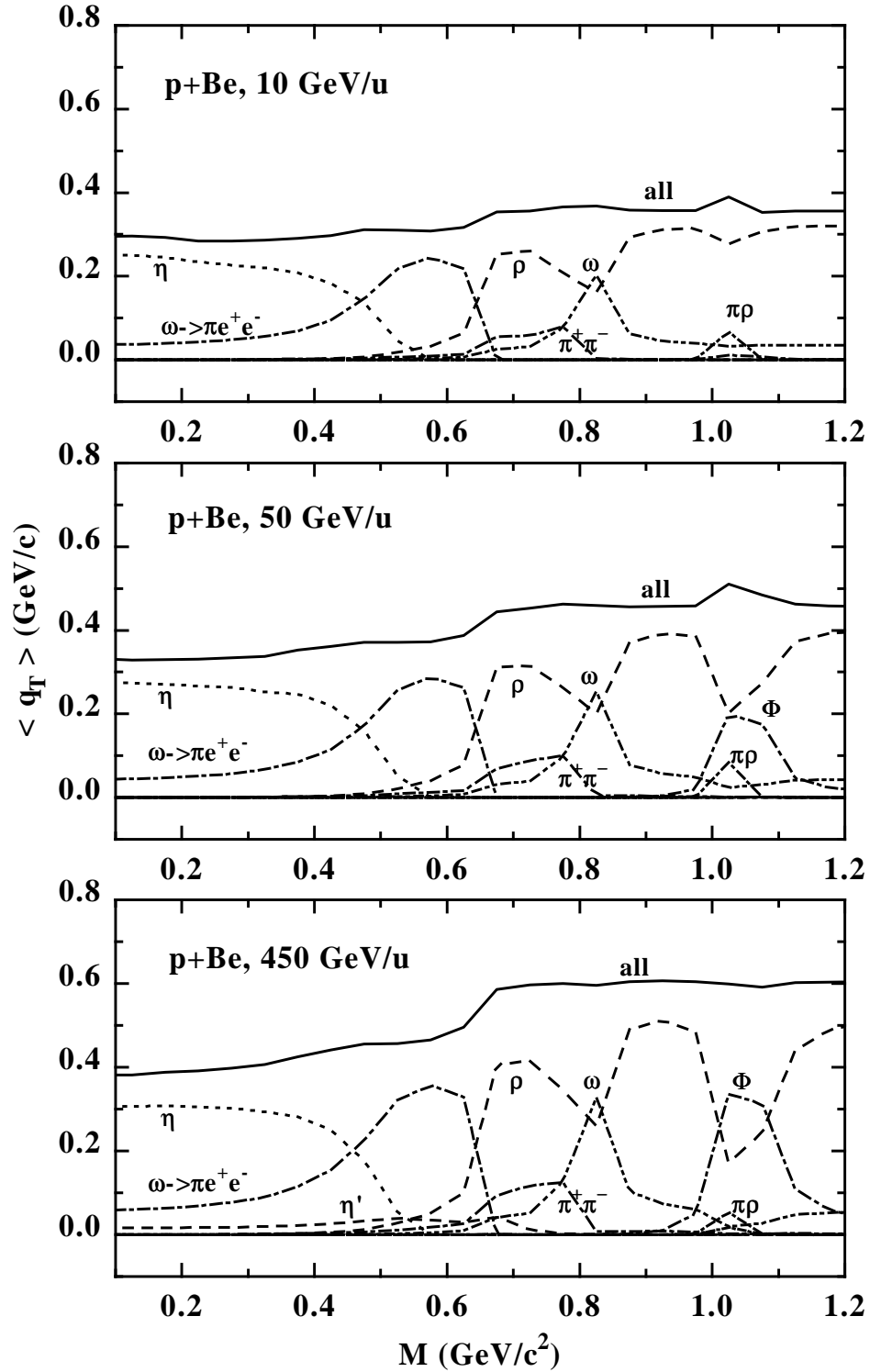
Figure 15: The average transverse momentum $< q_T > (M)$ including the channel decomposition for p + Be at 10, 50 and 450 GeV. The assignment of the individual contributions is the same as in Fig. 4.
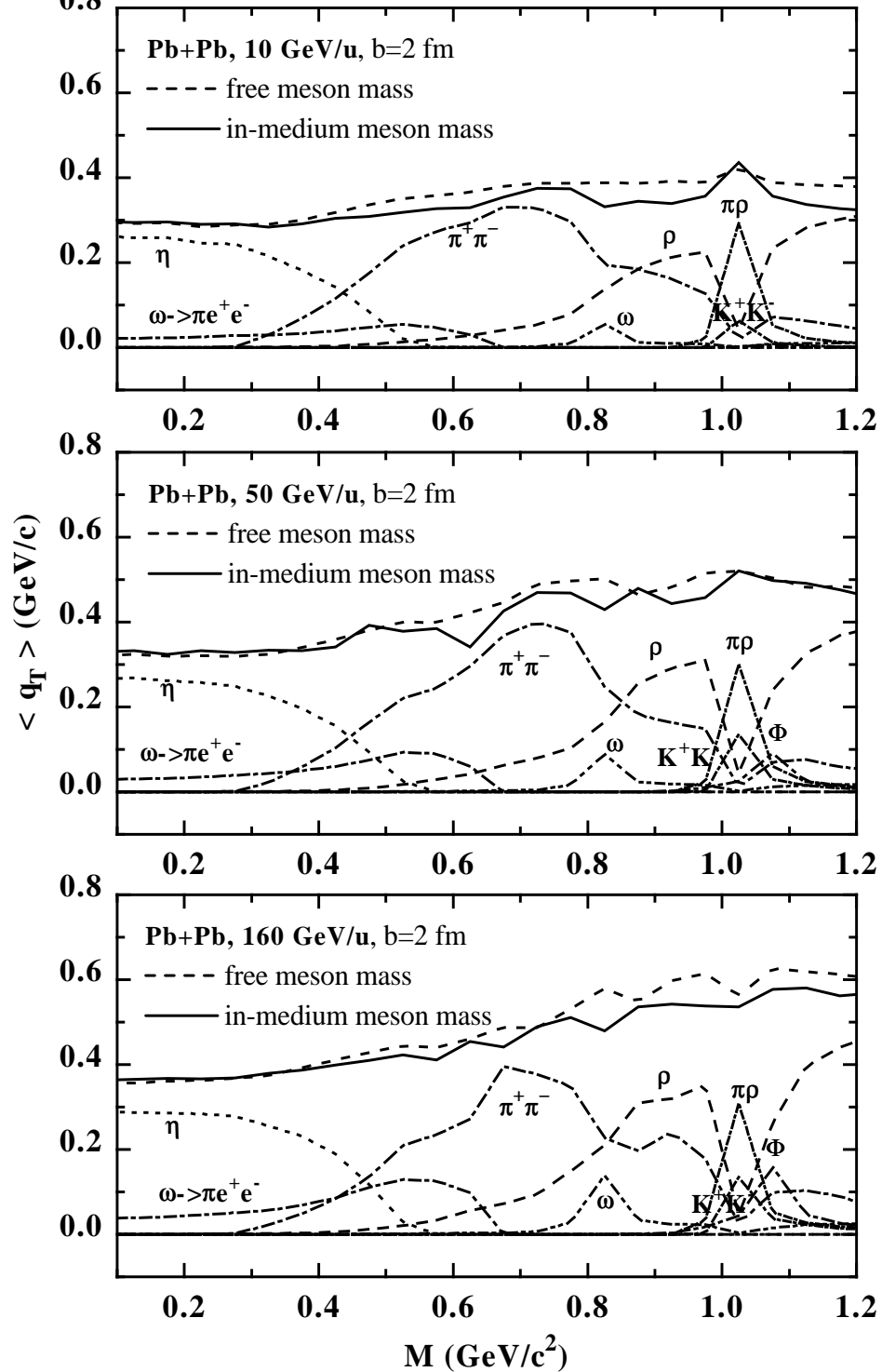
34

Figure 16: The average transverse momentum $< q_T > (M)$ including the channel decomposition for Pb + Pb at 10, 50 and 160 GeV/u at $b = 2$ fm without (dashed lines) and with in-medium meson mass modification (solid lines). The assignment of the individual contributions is the same as in Fig. 4.
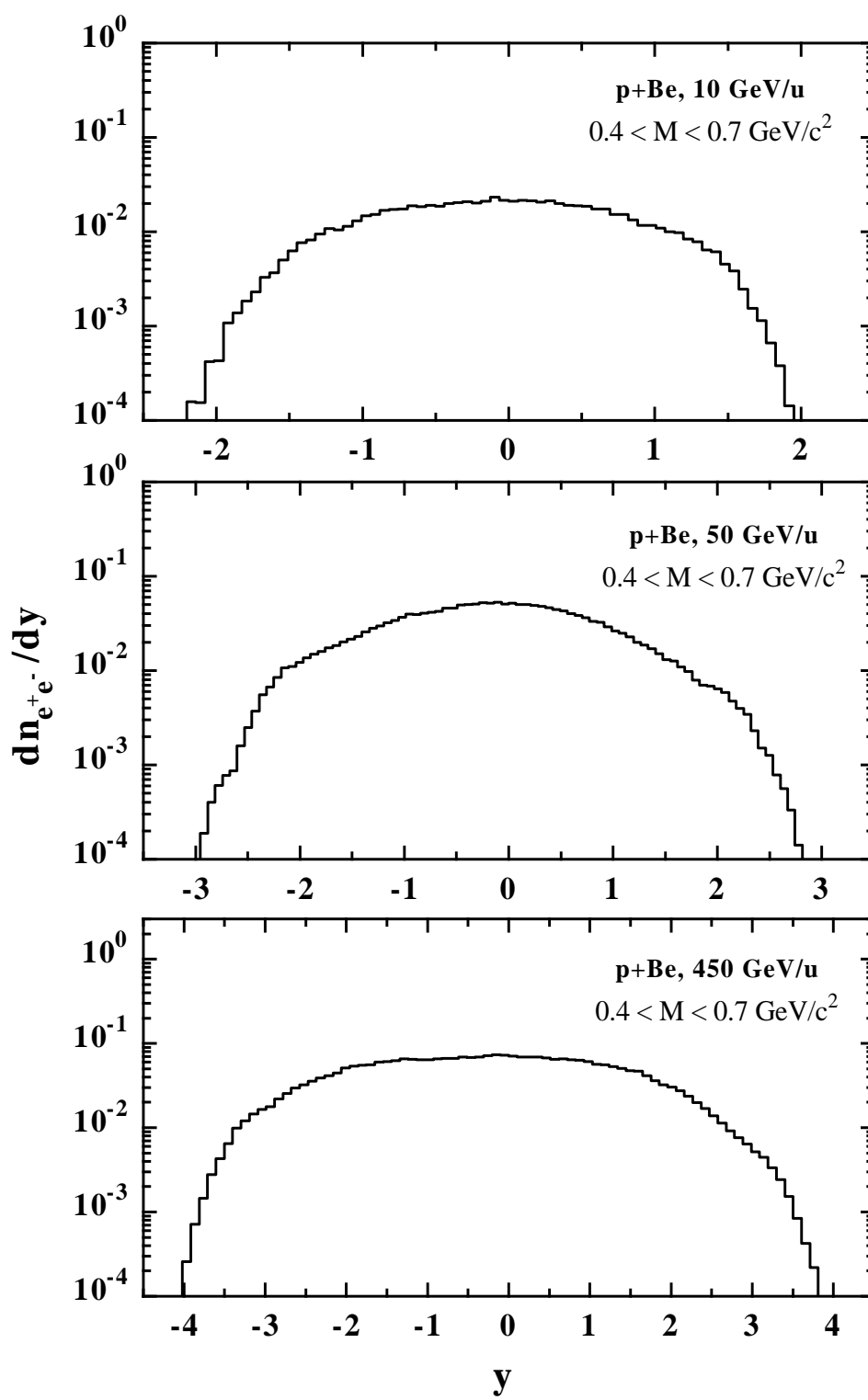
Figure 17: The dilepton rapidity distribution for the invariant mass range $0.4 \leq M \leq 0.7$ GeV for p + Be at 10, 50, and 450 GeV.
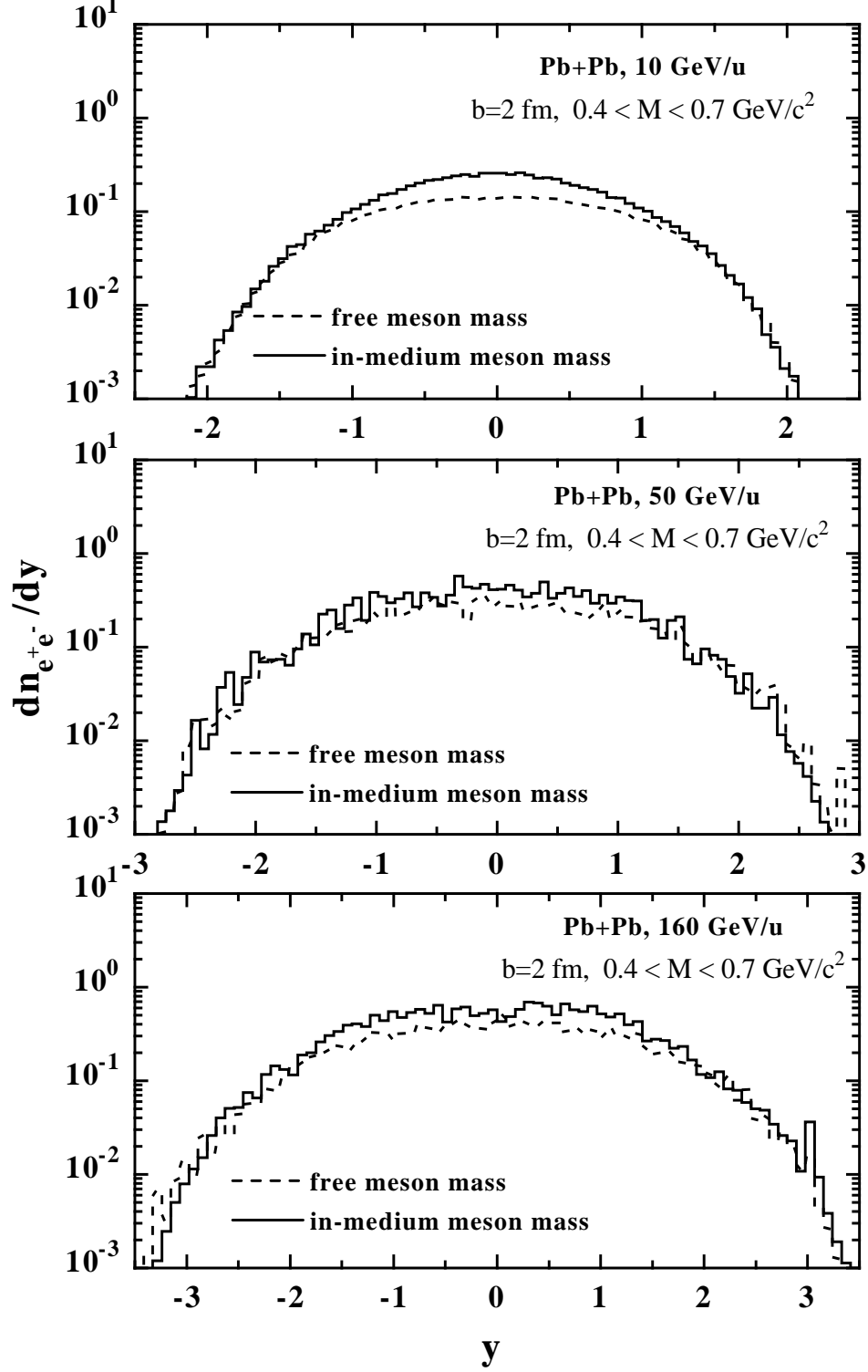
Figure 18: The dilepton rapidity distribution for the invariant mass range $0.4 \leq M \leq 0.7$ GeV for Pb + Pb at 10, 50 and 160 GeV/u at $b = 2$ fm without (dashed lines) and with in-medium meson mass modification (solid lines).
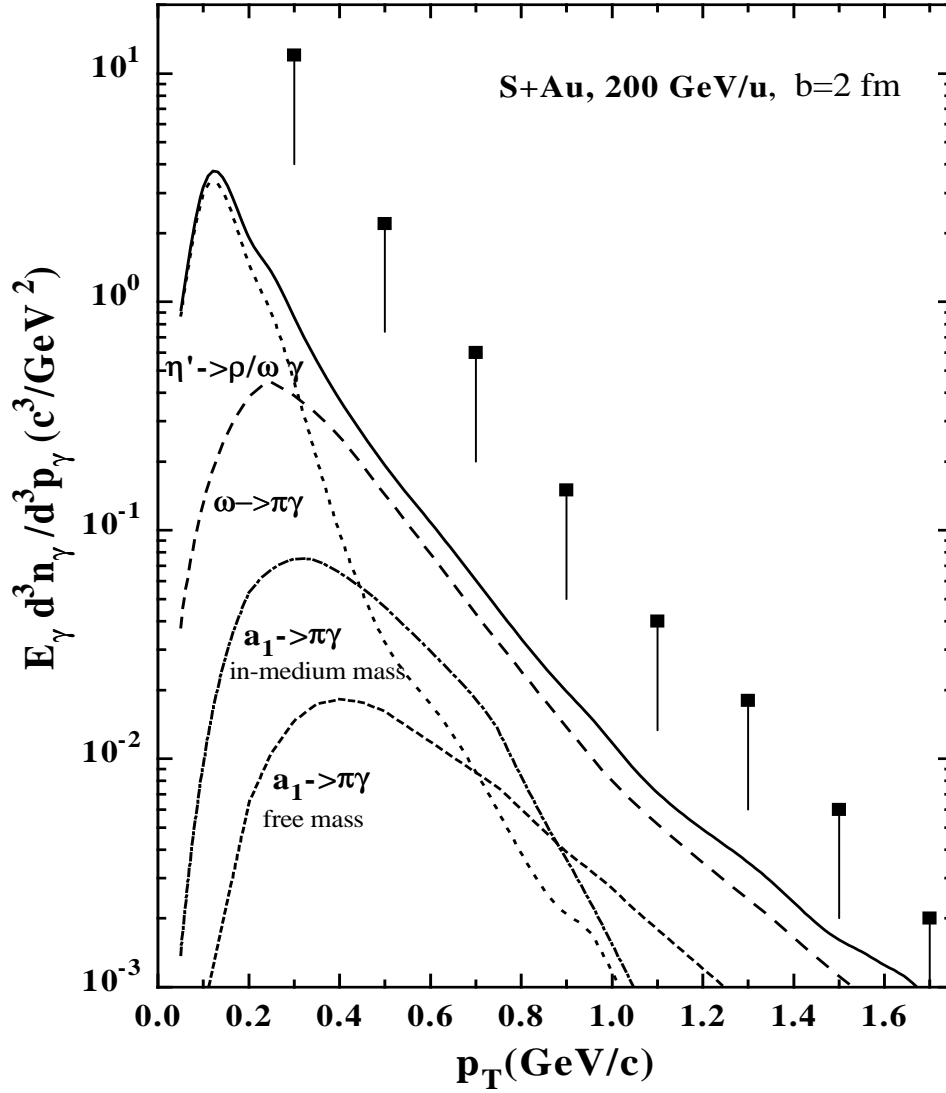
Figure 19: The differential photon multiplicity for central S + Au collisions at 200 GeV/u in comparison to the upper limits from the WA80 collaboration [49]; all contributions (solid line).